The stabilized supralinear network accounts for the contrast dependence of visual cortical gamma oscillations

Caleb J. Holt[1a], Kenneth D. Miller[2] and Yashar Ahmadian[3,1b]

[1a]Institute of Neuroscience, Department of Physics, University of Oregon, OR, USA
[1b]Institute of Neuroscience, Departments of Biology and Mathematics, University of Oregon, OR, USA
[2]Center for Theoretical Neuroscience, Swartz Program in Theoretical Neuroscience, Kavli Institute for Brain Science, and Dept. of Neuroscience, College of Physicians and Surgeons and Morton B. Zuckerman Mind Brain Behavior Institute, Columbia University, NY, USA
[3]Computational and Biological Learning Lab, Department of Engineering, University of Cambridge, Cambridge, UK

May 23, 2022

Summary

When stimulated, neural populations in the visual cortex exhibit fast rhythmic activity with frequencies in the gamma band (30-80 Hz). The gamma rhythm manifests as a broad resonance peak in the power-spectrum of recorded local field potentials which exhibits various stimulus dependencies. In particular, in macaque primary visual cortex (V1), the gamma peak frequency increases with increasing stimulus contrast. Moreover, this contrast dependence is local: when contrast varies smoothly over visual space, the gamma peak frequency in each cortical column is controlled by the local contrast in that column's receptive field. No parsimonious mechanistic explanation for these contrast dependencies of V1 gamma oscillations has been proposed. The stabilized supralinear network (SSN) is a mechanistic model of cortical circuits that has accounted for a range of visual cortical response nonlinearities and contextual modulations, as well as their contrast dependence. Here, we begin by showing that a reduced SSN model lacking topography robustly captures the contrast dependence of gamma peak frequency, and provides a mechanistic explanation for this effect based on the observed non-saturating and supralinear input-output function of V1 neurons. Given this result, the local dependence on contrast can trivially be captured in a retinotopically extended SSN which lacks horizontal synaptic connections between cortical columns, as in that case the gamma peak in a cortical column would be independently set by that column's feedforward input. However, long-range horizontal connections in V1 are in fact strong, and contextual modulation phenomena such as surround suppression are known to be, in part, mediated by these connections. We thus explored whether a retinotopically organized SSN model of V1 with strong excitatory horizontal connections can exhibit both surround suppression and the local contrast dependence of gamma peak frequency. We found that such a SSN can account for both effects, but only when the excitatory projections are composed of two components with different patterns of spatial fall-off with distance: a short-range component which only targets the source column, combined with a long-range component that targets columns neighboring the source column. We thus make a specific qualitative prediction for the spatial structure of horizontal connections in macaque V1, consistent with the columnar structure of cortex.

When presented with a stimulus, populations of neurons within visual cortices exhibit elevated rhythmic activity with frequencies in the so-called gamma band (30-80 Hz) (Jia et al., 2013; Ray and Maunsell, 2010). These gamma oscillations can be observed in local field potential (LFP) or electroencephalogram (EEG) recordings and, when present, manifest as peaks in the LFP/EEG power-spectra. It has been proposed that gamma oscillations perform key functions in neural processing such as feature binding (Singer, 1999), dynamic communication between cortical areas (Fries, 2005, 2015; Ni et al., 2016), or as a timing or "clock" mechanism that can enable coding by spike timing (Buzsáki and Chrobak, 1995; Draguhn and Buzsáki, 2004; Fries et al., 2007; Hopfield, 2004; Jefferys et al., 1996). These proposals, however, remain controversial (Ray and Maunsell, 2010).

While the computational role of gamma rhythms is not fully understood, much is known about their phenomenology. For example, defining characteristics of gamma oscillations, such as the width and height of the spectral gamma peak, as well as its location on the freqeuncy axis (peak frequency), exhibit systematic dependencies on various stimulus parameters (Gieselmann and Thiele, 2008; Henrie and Shapley, 2005; Jia et al., 2013; Ray and Maunsell, 2010). In particular, in the primary visual cortex (V1) of macaque monkeys, the power-spectrum gamma peak moves to higher frequencies as the contrast of large and uniform grating stimuli is increased (Jia et al., 2013; Ray and Maunsell, 2010). This establishes a monotonic relationship between gamma peak frequency and the grating contrast. We will refer to this contrast-frequency relationship, obtained using a grating stimulus with uniform contrast, as the "contrast dependence" of gamma peak frequency.

Moreover, when animals are presented with a stimulus whose contrast smoothly varies over the visual field (and hence over nearby cortical columns in V1), it is the local stimulus contrast that determines the peak frequency of gamma oscillations (Ray and Maunsell, 2010). Specifically, Ray and Maunsell 2010 used a Gabor stimulus (which has smoothly decaying contrast with increasing distance from the stimulus center), and found that the gamma peak frequency of different V1 recording sites match the predictions resulting from the frequency-contrast relationship obtained from the uniform grating experiment, but using the local Gabor contrast in that site's receptive field. We refer to this second effect as the "local contrast dependence" of gamma peak frequency.

It is well-known that networks of excitatory and inhibitory neurons with biological neural and synaptic time-constants can exhibit oscillations with frequency in the gamma band (*e.g.*, Brunel and Wang 2003; Tsodyks et al. 1997; see Buzsáki and Wang 2012 for a review). However, no mechanistic circuit model of visual cortex has been proposed which can robustly and comprehensively account for the contrast dependence of gamma oscillations. Jia et al. 2013 did propose a rate model that accounts for the increase of gamma peak frequency with increasing global contrast. However, their treatment only models the interactions between a single excitatory and a single inhibitory population, which is sufficient for spatially uniform stimuli, but cannot explain the local nature of the gamma peak frequency's contrast dependence. Moreover, even in the case of a uniform-contrast stimulus, this model could only produce very weak contrast-dependence of peak frequency, and moreover required a contrast-dependent scaling of the intrinsic time-constant of excitatory neurons. Here, we develop a parsimonious and self-contained mechanistic model (with fixed neural and network parameters) which accounts for the global as well as local contrast dependence of the gamma peak.

It is not clear how the local nature of the contrast-dependence of gamma oscillations can be reconciled with key features of cortical circuits. This locality would trivially emerge if cortical columns were non- or weakly interacting; in that case each column's oscillation properties would clearly be determined by its feedforward input (controlled by the local contrast). However, nearby cortical columns do interact strongly via the prominent horizontal connections connecting them (Gilbert and Wiesel, 1989). These interactions manifest, *e.g.*, in contextual modulations of V1 responses, such as in surround suppression (Cavanaugh et al., 2002), which are known to be partly mediated by horizontal connections (Schwabe et al., 2010).

Surround suppression is the phenomena wherein stimuli outside the classical receptive field (RF) of V1 neurons, which by themselves cannot drive the cell to respond, nevertheless modulate the cells' response, typically by suppressing it. Surround suppression results in a non-monotonic "size tuning curve", which is obtained by measuring a cell's response to circular gratings of varying sizes centered on that cell's RF: the response first increases with increasing stimulus size, but then decreases as the grating increasingly covers regions surrounding the RF. It is unclear whether a model of V1, featuring bi-

ologically plausible horizontal connections, can capture both surround suppression and the local contrast dependence of gamma oscillations.

A parsimonious, biologically plausible model of cortical circuitry which has successfully accounted for a range of cortical contextual modulations and their contrast dependence is the stabilized supralinear network (SSN) (Ahmadian et al., 2013a; Rubin et al., 2015). In particular, the SSN robustly captures the contrast dependencies of surround suppression, such as the observation that with increasing stimulus contrast size tuning curves peak at lower stimulus sizes (Rubin et al., 2015). Being a recurrently connected firing rate model with excitatory and inhibitory neurons, we expect the SSN to be able to exhibit oscillations similar to gamma rhythms. However, as pointed out previously, to capture fast dynamical phenomena, and in particular the gamma band resonance frequency, it is key to properly account for fast synaptic filtering as provided by the fast ionotropic receptors, AMPA and $GABA_A$ (Barbieri et al., 2014; Brunel and Wang, 2003; Ledoux and Brunel, 2011). We thus started by extending the SSN model to properly account for input currents through different synaptic receptor types, with different filtering timescales.

Gamma oscillations do not behave like sustained oscillations, as sustained oscillations display a sharp peak in the power spectrum, typically followed by trailing peaks at subsequent harmonics. Such oscillations would also be auto-coherent, *i.e.* have a consistent phase over several oscillation cycles. By contrast, gamma oscillations are not auto-coherent and their timing and duration vary stochastically (Burns et al., 2011, 2010), resulting in a single broad peak in the power-spectrum, with no visible higher harmonics (Jia et al., 2013; Ray and Maunsell, 2010), consistent with transient (damped) and noise-driven oscillations (Burns et al., 2011, 2010; Xing et al., 2012). We therefore studied the SSN in a regime where in the absence of time-dependent external inputs its firing rates reach a steady state, but when perturbed can exhibit damped oscillations with a characteristic frequency (technically, this means the network is close to, but below a Hopf bifurcation, *i.e.*, a transition to a regime of sustained oscillations). When perturbed by structureless noise that is sufficiently fast (the biological network's irregular spiking itself can provide such a noise source), these noise-driven damped oscillations manifest as a resonance peak in the power-spectrum of network activity (Kang et al., 2010; Xing et al., 2012).

We start Results section by developing an extension of the SSN that models the dynamics of input currents through different synaptic receptor types, with different timescales. We then study a reduced noise-driven SSN composed of two units representing excitatory (E) and inhibitory (I) sub-populations. We show that, for a wide range of biological parameters, this reduced SSN model generates gamma oscillations with peak frequency that robustly increases with increasing external drive to the network. We show that this robust contrast dependence is a consequence of a key feature of the SSN: the supralinear input-output (I/O) function of its neurons (which is known to fit well the non-saturating and expansive relationship between the firing rate and membrane voltage of V1 neurons (Anderson et al., 2000; Priebe and Ferster, 2008)). We next investigate the gamma peak's local contrast dependence using an expanded retinotopically organized SSN model of V1, with E and I units in different cortical columns. We show that this network is capable of reproducing the local contrast dependence of gamma peak frequency while exhibiting realistic surround suppression. However, as we show, this is only possible when the spatial fall-off of excitatory connection strengths has two distinct components: a sharp immediate fall across a cortical column's width, and a slower fall off that can range over several columns. This "local plus long-range" spatial structure of horizontal connections balances the trade-off between capturing local contrast dependence (requiring short-range or weak horizontal connections) and surround suppression (requiring the opposite). While achieving this balance requires a mild degree of parameter tuning, we show that it does not require fine-tuning of parameters and is robust to considerable parameter variations. In Methods, we present the details of the reduced and retinotopic models, the mathematical analyses, and numerical simulations. Finally, in the Discussion, we conclude by discussing the implications of our findings for the structure of cortical horizontal connections and the shape of neural input/output nonlinearities.

Results

Noise-driven SSN with multiple synaptic currents

As motivated in the introduction, and with the aim of modeling gamma oscillations, we started by extending the SSN model to properly account for synaptic currents through different receptor types with different kinetics.

In its original form, SSN's activity dynamics are governed by standard firing rate equations (Dayan and Abbott, 2001), in which each neuron is described by a single dynamical variable: either its output firing rate (Ahmadian et al., 2013b; Rubin et al., 2015) or its total input current (Hennequin et al., 2018). In the extended model, by contrast, each neuron will have more than one dynamical variable, corresponding to its input currents through different synaptic receptor types. Concretely, we will include the three main ionotropic synaptic receptors in the model: AMPA and NMDA receptors which mediate excitatory inputs, and $GABA_A$ (henceforth abbreviated to GABA) receptors which mediate the inhibitory input. For a network of N neurons, we will arrange these input currents to different neurons into three N-dimensional vectors, $\mathbf{h}^\alpha$, where $\alpha \in \{\text{AMPA}, \text{NMDA}, \text{GABA}\}$ denotes the receptor type. To model the kinetics of different receptors, we will ignore the very fast rise-times of all receptor types (as the corresponding timescales are much faster than the characteristic timescales of gamma oscillations), and only account for the receptor decay-times, which we denote by τ^α. With this assumption, the dynamics of $\mathbf{h}_t^\alpha$ are governed by (see Methods for a derivation)

$$\tau_\alpha \frac{d\mathbf{h}_t^\alpha}{dt} + \mathbf{h}_t^\alpha = W^\alpha \mathbf{r}_t + \mathbf{I}_t^\alpha \tag{1}$$

where $\mathbf{r}_t$ is the vector of firing rates, $W^\alpha \mathbf{r}_t$ and $\mathbf{I}_t^\alpha$ denote the recurrent and external inputs to the network mediated by receptor α, respectively, and W^α are $N \times N$ matrices denoting the contributions of different receptor-types to recurrent connectivity weights (the total recurrent connectivity weight matrix is thus given by $W = \sum_\alpha W^\alpha$). As in the cortex, the external input to the network is excitatory, and for simplicity we further assume that it only enters through AMPA receptors (*i.e.* $\mathbf{I}_t^\alpha$ is nonzero only for α = AMPA, and we will thus drop this superscript and denote this input by $\mathbf{I}_t$); including an NMDA components will not affect our results, as NMDA is slow relative to gamma band timescales. To close the system for the dynamical variables $\mathbf{h}_t^\alpha$, we have to relate the output rate of a neuron to its total input current. The fast synaptic filtering provided by AMPA and GABA allows for a static (or instantaneous) approximation to the input-output (I/O) transfer function of neurons (Brunel et al., 2001; Fourcaud and Brunel, 2002) (see Methods for further justification of this approximation):

$$\mathbf{r}_t = f(\mathbf{h}_t^{\text{total}}) = f\Big(\sum_\beta \mathbf{h}_t^\beta\Big), \tag{2}$$

where the I/O function $f(\cdot)$ acts element-wise on its vector argument. As in the original SSN, we take this I/O transfer function to be a supralinear rectified power-law, the key ingredient of SSN (see Fig. 1 A inset): $f(v) \equiv k[v]_+^n$, where k is a positive constant, $n > 1$ (corresponding to supralinearity), and $[x]_+ \equiv \max(0, x)$ denotes rectification. While the I/O function of biological neurons saturates at high firing rates (*e.g.*, due to refractoriness), throughout the natural dynamic range of cortical neurons firing rates stay relatively low. In fact, in V1 neurons the relationship between the firing rate and the mean membrane potential (an approximate surrogate for the neuronffs mean input) shows no saturation throughout the entire range of firing rates driven by visual stimuli, and is well approximated by a supralinear rectified power-law (Anderson et al., 2000; Priebe and Ferster, 2008).

Two-population model

We start by studying a reduced two-population model of V1 consisting of two units (or representative mean-field neurons): one excitatory and one inhibitory unit, respectively representing the excitatory and inhibitory neural sub-populations in the retinotopically relevant region of V1 (Fig. 1 A). This reduced model is appropriate for studying conditions in which the spatial profile of the activity is irrelevant, *e.g.*, when the grating stimulus is very large in size and we can assume the relevant V1 network is uniformly activated by the stimulus. Both units receive external inputs, and make reciprocal synaptic connections with each other as well as themselves.

As pointed out in the introduction, empirical evidence is most consistent with visual cortical gamma oscillations resulting from noise-driven fluctuations, and not from sustained coherent oscillations (Burns et al., 2011, 2010; Kang et al., 2010; Xing et al., 2012). To model such noise-driven oscillations using the SSN, as in (Hennequin et al., 2018), we assumed the external input consists of two terms $\mathbf{I}_t = \mathbf{I}_{DC} + \boldsymbol{\eta}_t$, where $\mathbf{I}_{DC}$ represents the stimulus drive to the network (by a steady time-independent stimulus), and $\boldsymbol{\eta}_t$ represents the stochastic noise input to the network. This input noise could be attributed to several sources, including sources that are (biologically) external or internal to V1. External noise can originate upstream in the lateral geniculate nucleus (LGN) of thalamus, or in feedback from higher areas. Internally generated noise results from the network's own irregular spiking (not ex-

plicitly modeled) which survives mean-field averaging as a finite-size effect (given the finite size of the implicitly-modeled spiking neuron sub-populations underlying the SSN's units). For simplicity, we assumed noise statistics are independent of stimuli, and thus of contrast. (Internal spiking noise is expected to have power that grows with the emerging firing rates in the network, as in a Poisson process. Since we are not interested in modeling changes in the gamma power –as opposed to peak frequency– with increasing contrast, we ignored this scaling, as it would not qualitatively affect the contrast dependence of peak frequency.) More specifically, we assumed that noise inputs to different neurons are independent, and each component is temporally correlated pink noise with a correlation time on the order of a few milliseconds (our main results are robust to changes in this parameter).We assume the strength of the feedforward input $\mathbf{I}_{DC}$ is proportional to the contrast of the visual stimulus.

For the first results shown in Fig. 1, we directly simulated the stochastic Eq. (1). Fig. 1C (dots) shows the average firing rates found in these simulations, and their contrast-dependence. The LFP signal is thought to result primarily from inputs to pyramidal cells, as they have relatively large dipole moments (Einevoll et al., 2013); we therefore took the net input to the E sub-population to represent the LFP signal. Fig. 1B shows examples of raw simulated LFP traces for different stimulus contrasts. For high enough contrast (including all nonzero contrasts shown), the LFP signal exhibits oscillatory behavior. These oscillations can be studied via their power-spectra (Fig. 1E, dots; see Methods). As Fig. 1F shows, the peak frequencies of the simulated LFP power-spectra shift to higher frequencies with increasing contrast. The two-population SSN model thus captures the empirically observed contrast dependence of gamma peak frequency (compare Fig. 1F with Fig. 1-I of Ray and Maunsell 2010 reproduced here as Fig. 1D).

To understand this behavior better, we employed a linearization scheme for calculating the LFP power-spectra. The linearization method allows for faster numerical computation of the LFP power-spectra, without the need to simulate the stochastic system Eq. (1). More importantly, the linearized framework allows for analytical approximations and insights, which as we show below, elucidate the mechanism underlying the contrast dependence of the gamma peak. We thus explain this approximation with some detail here (see Methods for further details). In any stimulus condition (corresponding to a given $\mathbf{I}_{DC}$), we first find the network's steady state in the absence of noise, by numerically solving the noise-free version of Eq. (1) (without linearization). The corresponding fixed-point equations can be simplified if we sum them over α, and define $\mathbf{h}_* \equiv \sum_\alpha \mathbf{h}_*^\alpha$ and $\mathbf{I}_{DC} \equiv \sum_\alpha \mathbf{I}_{DC}^\alpha$. We then arrive at the same fixed-point equation for $\mathbf{h}_*$ as in the original SSN (Ahmadian et al., 2013a):

$$\mathbf{h}_* = Wf(\mathbf{h}_*) + \mathbf{I}_{DC}. \tag{3}$$

After numerically finding $\mathbf{h}_*$, we then expand Eq. (1) to first order in the noise and noise-drive deviations around the fixed point, $\delta\mathbf{h}_t^\alpha \equiv \mathbf{h}_t^\alpha - \mathbf{h}_*^\alpha$, to obtain

$$\tau_\alpha \frac{d\delta\mathbf{h}_t^\alpha}{dt} = -\delta\mathbf{h}_t^\alpha + \tilde{W}^\alpha \sum_\beta \delta\mathbf{h}_t^\beta + \boldsymbol{\eta}_t^\alpha \tag{4}$$

where we defined

$$\tilde{W}^\alpha \equiv W^\alpha \,\mathrm{diag}\big(f'(\mathbf{h}_*)\big)\,, \tag{5}$$

where $f'(\mathbf{h}_*)$ denotes the vector of gains (slopes) of the I/O functions of different neurons at the operating point $\mathbf{h}_*$ (see the red tangent lines in Fig. 1 A inset). As we explain in the next subsection, the neural gains and their dependence on the operating point rates (themselves dependent on the stimulus $\mathbf{I}_{DC}^\alpha$, via Eq. (3)) play a crucial role in the contrast dependence of gamma peak frequency in the SSN.

Technically, the linear approximation is valid for small noise strengths, but we found that for the noise levels that elicited fluctuations with realistic sizes, the approximation was very good. As shown in Fig. 1E-F, the LFP power-spectra and their peak frequencies obtained using the linear approximation agree very well with those estimated from the direct stochastic simulations of Eq. (1). The firing rates of E and I units at the fixed-point solution Eq. (3) also provide a very good approximation to their mean steady-state rates, at different contrasts, as obtained from direct stochastic simulations of Eq. (1) (Fig. 1C). Below, we will thus calculate all power-spectra using the computationally much faster linear approximation, instead of stochastic simulations of Eq. (1).

Robustness of the two-population model

To demonstrate that the SSN robustly produces the contrast dependence of gamma peak frequency, we simulated 1000 different instances of the 2-population network with randomly drawn parameters. The sampled parameters were the weights of the connections between

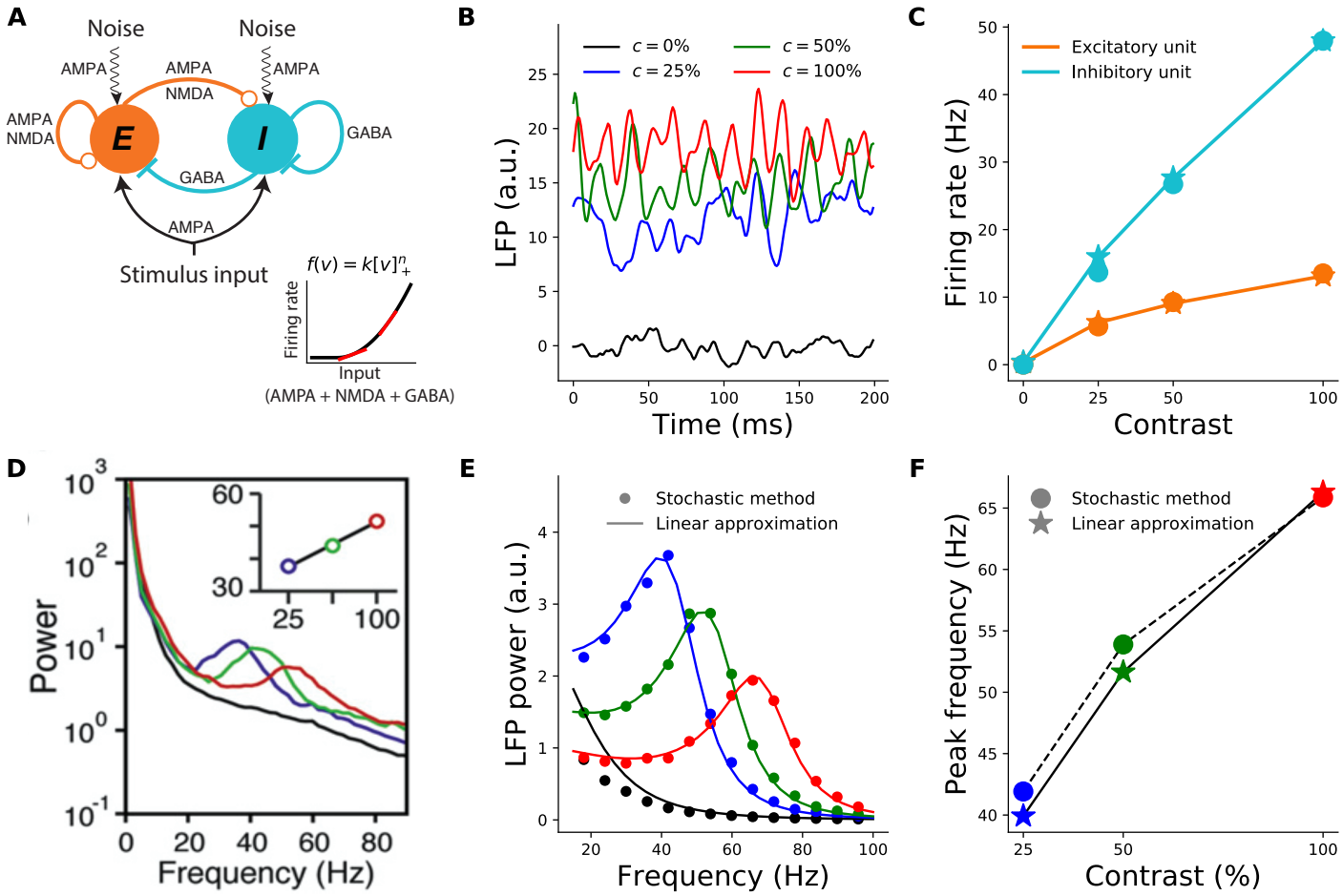

Figure 1. Contrast dependence of the gamma peak frequency in the 2-population model. **A:** Schematic of the 2-population Stabilized Supralinear Network (SSN). Excitatory (E) connections end in a circle; inhibitory (I) connections end in a line. Each unit represents a sub-population of V1 neurons of the corresponding E/I type. Both receive noisy input from the stimulus. **Inset:** The rectified power-law Input/Output transfer function of SSN units (black). Red lines indicate the slope of the I/O function at particular locations. **B:** Local field potential (LFP) traces, modeled as total net input to the E unit, from the stochastic model simulations under four different stimulus contrasts (c): 0% (black) equivalent to no stimulus or spontaneous activity, 25% (blue), 50% (green), 100% (red). The same color scheme for stimulus contrast is used throughout the paper. **C:** Mean firing rates of the excitatory (orange) and inhibitory (cyan) units as a function of contrast, from the stochastic simulations (dots) and linearized approximation (stars). Note that the dots and stars closely overlap. **D:** Reproduction of figure 1I from (Ray and Maunsell, 2010) showing the average of experimentally measured LFP power-spectra in Macaque V1. The inset shows the dependence of gamma peak frequency on the contrast of the grating stimulus covering the recording site's receptive field. **E:** LFP power-spectra for c = 0%, 25%, 50%, 100% (black, blue, green, and red curves, respectively) calculated from the noise-driven stochastic SSN simulations (dots), or using the linearized approximation (solid lines). **F:** Gamma peak frequency as a function of contrast, obtained from power-spectra calculated using stochastic simulations (dots and dashed line) or the linearized approximation (stars and solid line).

the two units ($E \to I$, $I \to E$) and their self-connections ($E \to E$, $I \to I$), the relative strength of input to the excitatory and inhibitory units, and the NMDA fraction of excitatory synaptic weights.

The obtain a parameter-set, we first sampled the mentioned parameters uniformly at random from a biologically plausible range (see Methods). Individual parameters were first sampled independently, but we rejected a parameter-set if it the corresponding noise-free SSN

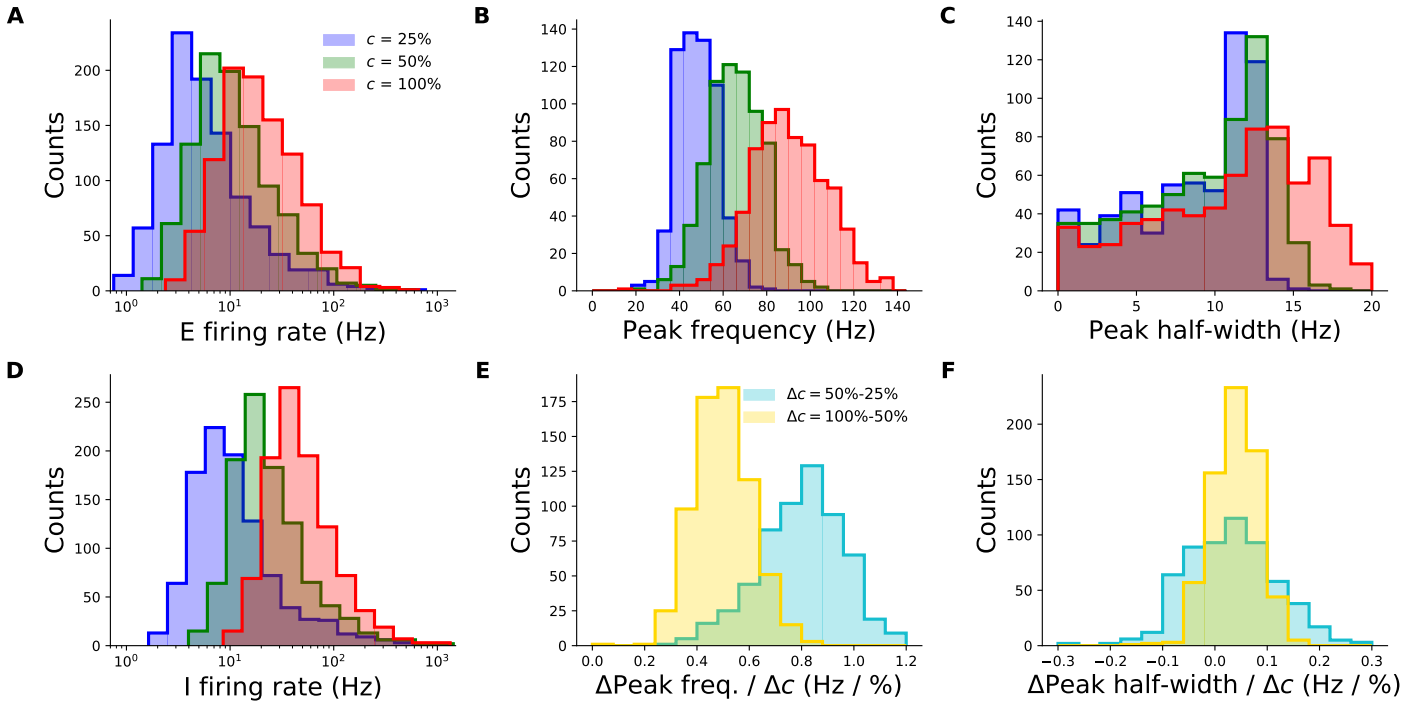

Figure 2. Robustness of the contrast-dependence of gamma peak frequency to network parameter variations. One thousand 2-population SSN's were simulated with randomly sampled parameters, and all histograms show simulation counts. **A:** Distributions of the excitatory unit's firing rate in response to 25%, 50%, and 100% contrast stimuli (blue, green, red), plotted on a logarithmic scale. 100% of networks shown across all contrasts. **B:** Distributions of the gamma peak frequencies at different stimulus contrasts. 60.9%, 50%, 50% of networks had gamma peaks at 25% (blue), 50% (green), and 100% (red) contrast respectively. **C:** Distributions of the gamma peak widths at different stimulus contrasts. **D:** Same as panel A, but for the inhibitory unit. 100% of networks shown across all contrasts. **E:** Distributions of the change in gamma peak-frequency normalized by the change in stimulus contrast, either 25% and 50% (cyan - 35.8% of networks) or 50% and 100% (yellow - 48.4%). **F:** Same as panel **E**, but for gamma peak-width.

did not reach a stable fixed point for all studied input contrasts (this corresponds to our modelling choice to have the SSN in a damped oscillation regime). We also discarded parameter-sets for which the excitatory firing rates would exhibit non-monotonic dependce on contrast (using an inequality criteria derived in (Ahmadian et al., 2013a); see Methods for details).

By and large, our simulations of randomly sampled 2-population SSN models produced fixed-point firing rates for both the excitatory and inhibitory units that were within the biologically plausible window of values, across all contrasts (Fig. 2A and D). Furthermore, many two-population networks produced peak frequencies that are within the gamma band (30 - 80 Hz) for all contrast conditions, though some produced peaks at higher frequencies for the higher contrasts (Fig. 2 B). The distributions also shift towards higher frequencies with increasing contrast, suggesting that the two-population SSN is indeed able to robustly reproduce the contrast dependence of gamma peak frequency. To demonstrate this more directly, we show the distributions of the changes in peak frequency normalized by the change in contrast in Fig. 2E. None of the sampled networks produced negative changes in peak frequency for positive changes in the stimulus contrast.

As a further corroboration of our model, we also studied how the width of the gamma peak changed with increasing contrast. While (Jia et al., 2013; Ray and Maunsell, 2010) did not quantify changes in their gamma peak width with increasing contrast, their results suggest that no significant systematic change in width was observed (Fig. 1 D). Similarly, in our two-population network, changes in the half-width of the gamma peak are relatively small, and the direction of change can be positive or negative with similar probability (Fig. 2 F).

Mechanism underlying the contrast dependence of gamma peak frequency

As we will now show, the SSN sheds light on the mechanism underlying the contrast dependence of the gamma peak, and specifically pins it to the expansive supralinear nature of the neuronal I/O transfer function. This also explains the robustness of the effect to changes in connectivity and external input parameters as demonstrated in the previous subsection.

In the linearized approximation, the LFP power-spectrum (see Eqs. (23)–(25) in Methods) can be expressed in terms of the so-called Jacobian matrix, *i.e.* the matrix of couplings of the dynamical variables, $\delta \mathbf{h}_t^\alpha$, in the linear system Eq. (4); thus, for a network of N neurons, the Jacobian is a $3N \times 3N$ matrix, or 6×6 in the two-population model. The existence of damped oscillations and the value of their frequency (which is the resonance frequency manifesting as a peak in the power-spectrum) are in turn determined by the existence and the imaginary part value of a complex eigenvalue of the Jacobian matrix. Previously, the eigenvalues of the Jacobian for a standard *E-I* firing rate network, without different synaptic current types, were analyzed by Tsodyks et al. 1997, and conditions for emergence of (damped or sustained) oscillations were found. In Appendix 1, we show that, given the slowness of NMDA receptors relative to gamma timescales, the effect of NMDA receptors on the complex eigenvalues of the Jacobian can be safely ignored, and as a result, only two (out of 6) eigenvalues of the resulting Jacobian can become complex (and thus able to create a gamma peak). Moreover, this pair (which we denote by $\lambda_\pm$) correspond to the two eigenvalues of a standard *E-I* rate model (Tsodyks et al., 1997) whose *E* and *I* neural time-constants are given, respectively, by the AMPA and GABA decay times:

$$2\lambda_\pm = \gamma_E(\tilde{W}_{EE} - 1) - \gamma_I(\tilde{W}_{II} + 1) \pm \sqrt{\left[\gamma_E(\tilde{W}_{EE} - 1) + \gamma_I(\tilde{W}_{II} + 1)\right]^2 - 4\gamma_E\gamma_I\tilde{W}_{EI}\tilde{W}_{IE}} \quad (6)$$

where $\gamma_E = \tau_{\text{AMPA}}^{-1}$ and $\gamma_I = \tau_{\text{GABA}}^{-1}$. Here we defined

$$\tilde{W}_{ab} \equiv W_{ab} f'(h_a^*) \qquad (a, b \in \{E, I\}), \quad (7)$$

where $W_{ab} \equiv \sum_\alpha W_{ab}^\alpha$ is the total synaptic weight from unit b to unit a, and (as in Eq. (5)) $f'(h_a^*)$ is the gain of unit a, *i.e.* the slope of its I/O function, at the operating point set by the stimulus. We refer to $\tilde{W}_{ab}$ as effective synaptic connection weights. Unlike raw synaptic weights, these effective weights are modulated by the neural gains, and thereby by the activity levels in the background fixed points and thus by the stimulus input which sets those.

As mentioned, (damped or sustained) oscillations emerge when the above eigenvalues are complex (in which case λ_+ and λ_- are complex conjugates). This happens when the expression under the radical in Eqn. 6 is negative, *i.e.*

$$4\gamma_E\gamma_I\tilde{W}_{EI}\tilde{W}_{IE} > \left[\gamma_E(\tilde{W}_{EE} - 1) + \gamma_I(\tilde{W}_{II} + 1)\right]^2. \quad (8)$$

Qualitatively, the left hand side of the above inequality is a measure of the strength of the effective negative feedback between the *E* and *I* sub-populations, while the right hand size is a measure of the positive feedback in the network (arising from the network's recurrent excitation and disinhibition). Oscillations thus emerge when the negative feedback loop between *E* and *I* is sufficiently strong, in the precise sense of Eqn. 8.

During spontaneous activity (when the external input is zero or very weak), the rates of both *E* and *I* populations are very small. This means that the spontaneous activity operating point sits near the rectification of the neuronal I/O transfer functions where the neural gains are very low (Fig. 1A left). Thus in the spontaneous activity state, the dimensionless effective connections are relatively small. In the limit of $\tilde{W}_{ab} \to 0$, the left hand side of Eqn. 8 goes to zero, while its right side goes to $(\gamma_I - \gamma_E)^2$ which is generically positive; hence the inequality is not satisfied. This shows that the spontaneous activity state generically does not exhibit oscillations, in agreement with lack of empirical observation of gamma oscillation during spontaneous activity.

On the other hand, when condition Eqn. 8 does hold, the frequency of the oscillations are given by the imaginary part of the eigenvalues, *i.e.*

$$\text{resonance frequency} = \frac{1}{2\pi}\sqrt{\gamma_E\gamma_I\tilde{W}_{EI}\tilde{W}_{IE} - \left[\gamma_E(\tilde{W}_{EE} - 1)/2 + \gamma_I(\tilde{W}_{II} + 1)/2\right]^2} \quad (9)$$

(the division by 2π is because the eigenvalue imaginary parts give the angular frequency). As we will discuss further below the resonance frequency (or approximately the gamma peak frequency [Fig. 3B]) thus depends on the effective connections weights and is thus modulated by the neural gains. (Note, however, that the *scale* or order of magnitude of this frequency is set by γ_E and γ_I, *i.e.*, by the decay times of AMPA and GABA, as the effective connection weights are dimensionless and cannot determine the dimensionful scale of the gamma frequency;

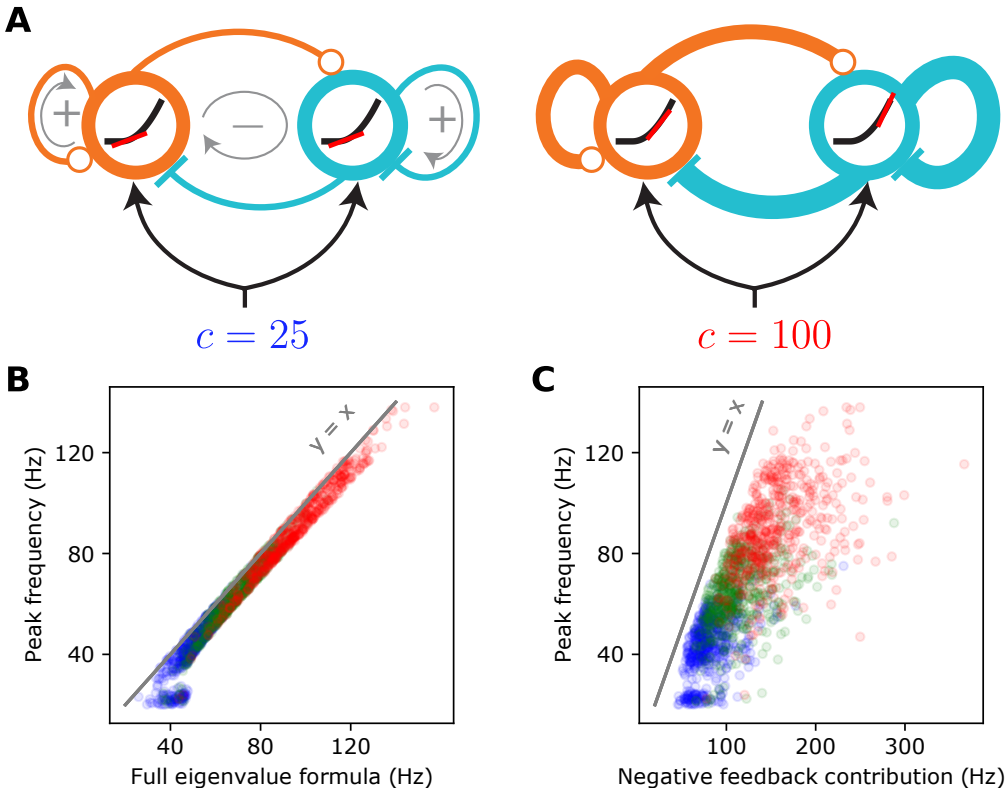

Figure 3. The supralinear nature of the neural transfer function can explain the contrast dependence of gamma frequency. **A:** Schematic diagrams of the 2-population SSN (see Fig. 1-A) receiving a low (left) or high (right) contrast stimulus. The thickness of connection lines represents the strength of the corresponding effective connection weight, which is the product of the anatomical weight and the input/ouput gain of the presynaptic neuron. The gain is the slope (red line) of the neural supralinear transfer function (black curve), shown inside the circles representing the *E* (orange) and *I* (cyan) units. A resonance frequency exists when the effective "negative feedback" (gray arrow enlcosing a minus sign) dominates the effective "positive feedback" (gray arrows enclosing positive signs), in the sense of the inequality Eq. (8). As the stimulus drive (c) increases (right panel), the neurons' firing rates in the network's operating point increase. As the transfer function is supralinear, this translates to a higher neural gains and stronger effective connections. When a resonance frequency already exists at the lower contrast, this strengthening of effective recurrent connections leads to an increase in the gamma peak frequency, approximately given by the imaginary part of the linearized SSN's complex eigenvalue, Eq. (6). **B:** The eigenvalue formula (9) provides an excellent approximation to the gamma peak frequency across sampled networks (see Fig. 2) and contrasts; correlation coefficient = 0.98 ($p < 10^{-6}$), for all data points combined across 25% (blue), 50% (green), and 100% (red) contrasts. **C:** The negative feedback loop contribution to the resonance frequency (Eq. (9) with the second term under the square root neglected) overestimates gamma peak frequency but is positively and significantly correlated with it; correlation coefficient = 0.75 ($p < 10^{-6}$).

ignoring the "positive feedback" contribution in Eq. (9), we find resonance frequency $\propto \sqrt{\gamma_E \gamma_I}/(2\pi)$, which for $\tau_{AMPA} \sim \tau_{GABA} \sim$ 4-6 ms, is on the order of 30-40 Hz.)

Equation (9) provides the insight into the contrast dependence of the gamma peak frequency (see Fig. 3). As contrasts increase the fixed-point firing rates increase (Fig. 1C). Because the SSN I/O transfer function is non-saturating and supralinear, as the rates increase the gains (*i.e.*, the slope of the I/O transfer functions) of the *E* and *I* cells are also guaranteed to increase (Fig. 3A right *vs.* left). The increase in the gains leads in turn to the strengthening of the effective connection weights, Eq. (7), and therefore of the network's negative *E*-*I* feedback loop. When Eq. (8) is satisfied, a rough approximation (Fig. 3B *vs.* C) to the resonance frequency is obtained by ignoring the positive feedback contribution (the second term under the

square root in Eq. (9)). With only the negative feedback contribution retained, it is clear that an increase in neural gains leads to an increase in the resonance frequency (the precise conditions for this to occur are given in Appendix 2 below). Thus as contrasts increase, we expect the gamma peak in the LFP power-spectrum to move to higher frequencies, due to increasing gains as dictated by the supralinear neural I/O transfer function.

Retinotopic SSN

We next investigated whether the SSN can account for the locality of contrast dependence of gamma peak frequency, when V1 receives a stimulus with a spatially varying contrast profile. To this end, we expanded our network from two units representing global E and I populations to many units that are retinotopically organized. We thus model the cortex as a two-dimensional grid which has an E and I sub-population (corresponding to SSN units) at each grid location corresponding to a cortical column (Fig. 4A). In the retinotopic SSN, the stimulus input can vary across the network: each column can receive a different input proportional to the contrast within its receptive field. We presented this network with uniform-contrast grating stimuli of various sizes and contrasts (the stimulus in Fig. 4A), as well as a Gabor stimulus (Fig. 4E) similar to the one used in Ray and Maunsell 2010, with a contrast profile that decays smoothly with deviation from the stimulus center, according to a Gaussian profile (see Eq. (??)).

We wish to study the trade-off in this model between capturing surround suppression of firing rates and capturing the local dependence of gamma peak frequency, and whether parameter choices exist for which the model can capture both of these effects. In particular, we will be studying the effect of the spatial profile of the horizontal recurrent connections between and within different cortical columns on this trade-off. In one extreme, we can consider a network in which long-range connections between different columns are very weak, and thus cortical columns are weakly interacting and can be approximated by independent two-population networks which were studied above (Figs. 1–1). In this case, the frequency of the gamma resonance in each column depends only on the gains and activity levels in that column, which are in turn set by the feedforward input to that column, controlled by the local stimulus contrast. Therefore a network with such a connectivity structure would trivially reproduce the local contrast-dependence of gamma peak frequency. However, due to lack of strong inter-columnar interactions, such a network would fail to to produce significant surround suppression of firing rates. In the other extreme, inter-columnar strengths are strong and, importantly, have a smooth fall-off (*e.g.* an exponential fall) with growing distance between pre- and post-synaptic columns; this is the case in most cortical network models, including the SSN model of (Rubin et al., 2015) that captures surround suppression and its various contrast-dependencies. However, as we will show below (Fig. 6), in such networks, when horizontal connections are strong enough to produce surround suppression, the gamma peak frequency is typically shared across all activated columns, regardless of the spatial contrast profile of the stimulus, and thus this connectivity structure cannot capture the local contrast-dependence of gamma peak frequency. Indeed, as shown below, within this class of networks (*i.e.*, those with a smooth spatial connectivity profile), we were not able to find connectivity parameters (controlling the range and strength of horizontal connections) for which the network could produce significant surround suppression and yet capture the local contrast-dependence of gamma (see Fig. 6 and the related subsection below).

We then asked whether connectivity structures which feature strong long-range connections, but in which local, intra-columnar connectivity is specially emphasized could produce both of these effects. In such a structure, the connection strength between two units first undergoes a sharp drop when the distance between the units exceeds the width of a column, and then falls off smoothly over a longer distance, possibly ranging over several columns. This modification can be thought of as adding a local, intra-columnar-only component to a connectivity profile with smooth fall-off. Specifically, we let the excitatory horizontal connections in our model have such a form. Denoting the strength of connection from the unit of type b at location $\mathbf{y}$ to the unit of type a at location $\mathbf{x}$ by $W_{\mathbf{x},a|\mathbf{y},b}$ (with $a, b \in \{E, I\}$), we thus chose:

$$W_{\mathbf{x},a|\mathbf{y},E} \propto \lambda_{a,E}\delta_{\mathbf{x},\mathbf{y}} + (1-\lambda_{a,E})e^{\frac{-\|\mathbf{x}-\mathbf{y}\|}{\sigma_{a,E}}} \qquad (a \in \{E, I\}), \tag{10}$$

where $\delta_{\mathbf{x},\mathbf{y}}$ (the local component) is the Kronecker delta: 1 when $\mathbf{x} = \mathbf{y}$ and zero otherwise. The $\lambda_{E,E}$ and $\lambda_{I,E}$ parameters lie between 0 and 1, and interpolate between the two extremes of connectivity structure: for $\lambda_{a,b} = 0$ the horizontal connectivity profile has only one spatial scale and

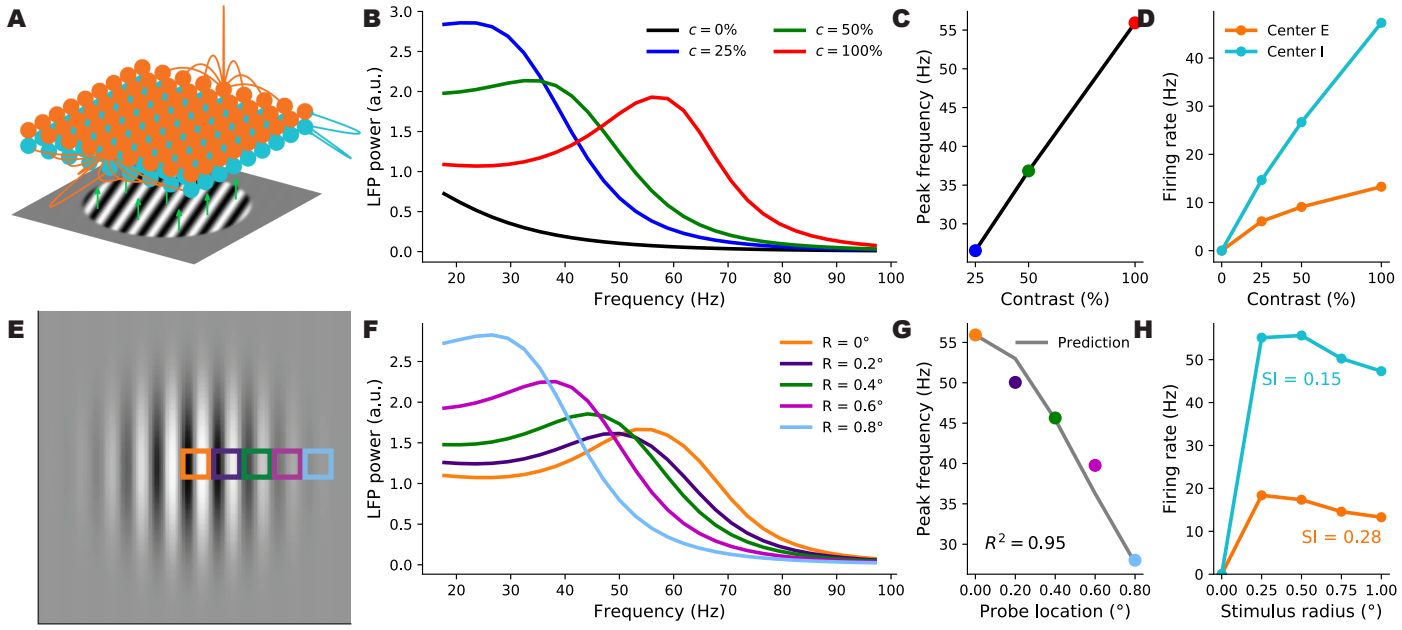

Figure 4. A retinotopically-structured SSN model captures the local contrast dependence of gamma peak-frequency, as well as the surround suppression of excitatory and inhibitory firing rates. **A:** Schematic of the retinotopic grid and inputs. At each location in retinotopic space, there exists an excitatory (orange) and inhibitory (cyan) sub-population which receives input (green arrows) from the stimulus (grating). Conenctions from excitatory units are shown in orange, while connections from inhibitory units are shown in cyan. **B:** LFP power-spectra of the excitatory center sub-population during different flat grating stimuli contrast, 0% (black), 25% (blue), 50% (green), and 100%. **C:** Peak frequency of the power-spectra gamma band under various flat grating contrast conditions. **D:** Fixed-point firing rates for the excitatory (orange) and inhibitory (cyan) sub-populations at the center of the retinotopic grid for increasing stimulus contrast. **E:** Representation of the Gabor input to the full retinotopic grid of units. Each square is colored according to the retinotopic receptive field of the sub-populations represented in the grid, 0° displaced from the center (orange), 0.2° (navy), 0.4° (green), 0.6° (magenta), and 0.8° (sky blue). **F:** Power-spectra of the excitatory sub-population colored according to distance displaced from the center of the grid. **G:** Gamma peak frequency of the power-spectra at increasing distance from the center of the grid. The gray curve shows a prediction of the displaced units' peak frequency given their local contrast based on the shift in gamma peak frequency of the center *E* sub-population as the contrast of a flat grating changes. **H:** Suppression curve of the firing rates. The firing rates of the center excitatory and inhibitory subpopulations vary non-monotonically as a flat grating stimulus is grown in size, and their suppression indices are 0.27 for the center *E* sub-population (orange), and 0.21 for the center *I* sub-population (cyan).

falls off smoothly with distance, while for $\lambda_{a,b} = 1$ connectivity is purely local and intra-columnar. The orange lines in Fig. 4A show examples of this connectivity profile. As in previous work (Rubin and Miller, 2010), we chose a smooth gaussian profile for inhibitory connections (see Eq. (32)), with a relatively short range (see the cyan lines in Fig. 4A).

In Fig. 4B-H, we show the behavior of firing rates and the gamma peak in one such network (with $\lambda_{E,E} = 0.4$ and $\lambda_{I,E} = 0.7$) in response to different stimuli. We first presented this network with flat gratings of varying sizes and contrasts, and measured the LFP power-spectrum and the firing rate responses of the *E* and *I* sub-populations at the "center" column, *i.e.*, at the retinotopic location on which the grating was centered. Firing rates of center *E* and *I* both increased with contrast (Fig. 4D), and for large enough gratings, we verified that the gamma peak frequency also increases with increasing contrast (Fig. 4B-C), matching the results of the reduced 2-population model and our previously built intuition. To study surround suppression, we formed the so-called size-tuning curve of the center *E* and *I* populations, based on their responses to full-contrast flat grat-

ings of different sizes (Fig. 4H). Both E and I responses showed surround suppression: the response first grows but then drops with increasing grating size. The center E sub-population had a suppression index (see Methods for the definition) of 0.28 consistent with biologically reported values of suppression indices (Gieselmann and Thiele, 2008).

To study the locality of contrast dependence, we modeled the experiment of Ray and Maunsell 2010, and presented this network with a Gabor stimulus, which has spatially varying contrast with a gaussian profile. We then computed the LFP spectrum at five locations ("columns") of increasing distance from the center of the Gabor stimulus (the colored squares in Fig. 4E) with the farthest one lying at 0.8 degrees of visual angle from the Gabor center (compare with the Gabor's σ which was 0.5° as in Ray and Maunsell 2010). The LFP power-spectra at all locations are shown in Fig. 4F. As seen, the gamma peak moves to lower frequencies with increasing distance from the Gabor center, which is accompanied by a decrease in the local contrast (*i.e.* the contrast of the Gabor stimulus at the receptive field location of the recording site). To quantify the locality of this contrast dependence, we again followed Ray and Maunsell 2010, by comparing the actual peak frequency at location $\mathbf{x}$ with a prediction that solely depended on the local contrast, $c(\mathbf{x})$, of the Gabor stimulus at $\mathbf{x}$. The prediction was the peak frequency of gamma recorded at the center location, when the network is presented with a large flat grating of (uniform) contrast equal to $c(\mathbf{x})$. We found that the prediction was in very close agreement with the actual peak frequencies at all distances (Fig. 4F). As a measure of the locality of gamma contrast-dependence, we used the corresponding coefficient of determination, R^2, which quantifies the agreement between the predicted and actual peak frequencies. (By definition, $R^2 = 1 - \frac{\text{SSE}}{\text{Var}}$, where SSE denotes the sum of squared differences between the predicted and the actual gamma peak frequencies, and Var denotes the variance of the latter; R^2 is thus bounded above by 1, which is attained when the prediction perfectly matches the actual data.) In the example shown in Fig. 4F, we found $R^2 = 0.95$.

To investigate whether the above behavior did or did not require fine tuning of network parameters, we simulated 500 networks with perturbed parameters around the parameters of the network shown in Fig. 4. Each parameter was drawn independently from a uniform distribution between -10% to 10% of that parameter's value in the network of Fig. 4 (rejection criteria were also applied after this step as in the samplings of the two-population model in Fig. 2 to ensure stable steady-states in the absence of noise; see Methods for details).

These networks produced biologically plausible and increasing center excitatory and inhibitory firing rates for changing contrasts (Fig. 5A and D, showing rates for the largest flat grating). The perturbed networks also robustly produce peak frequencies in the gamma band, that move upwards with increasing contrast (Fig. 5B and E, again showing gamma peak frequencies elicited by the largest flat grating). All these networks produced robust surround suppression with many realized networks showing higher suppression indices than the original unperturbed network (Fig. 5C). Finally, for each perturbed network, we again quantified the locality of contrast dependence of peak frequency, using the R^2 coefficient for the match between peak frequencies obtained at different recording location relative to the center of the Gabor stimulis and their predictions based on the local contrast and peak frequencies obtained using the flat grating with at that contrast. A dominant majority of our networks resulted in a high R^2 (larger than 0.8) signifying local contrast-dependence of gamma peak frequency (5F). In a minority of networks which did produce gamma peaks, however, the local prediction for peak frequency did not agree closely with the actual peak frequencies obtained using the Gabor stimulus.

In sum, the retinotopic SSN with the connectivity structure Eq. (10), which emphasizes the local intra-columnar excitation, can produce both the surround suppression of firing rates as well as the locality of contrast dependence of gamma peak frequency, without the need for fine tuning of its parameters.

Retinotopic SSN with a smooth fall-off of excitatory horizontal connectivity

As mentioned above, we were not able to find retinotopic SSN networks (such as the retinotopic model of Rubin et al. 2015) with a smooth horizontal connectivity spatial profile (in the notation of Eq. (10), we mean networks with $\lambda_{a,E} = 0$) which were able to both produce strong surround suppression and capture the local constrast-dependence of gamma peak frequency. Here we show the results of that search using random sampling of 1000

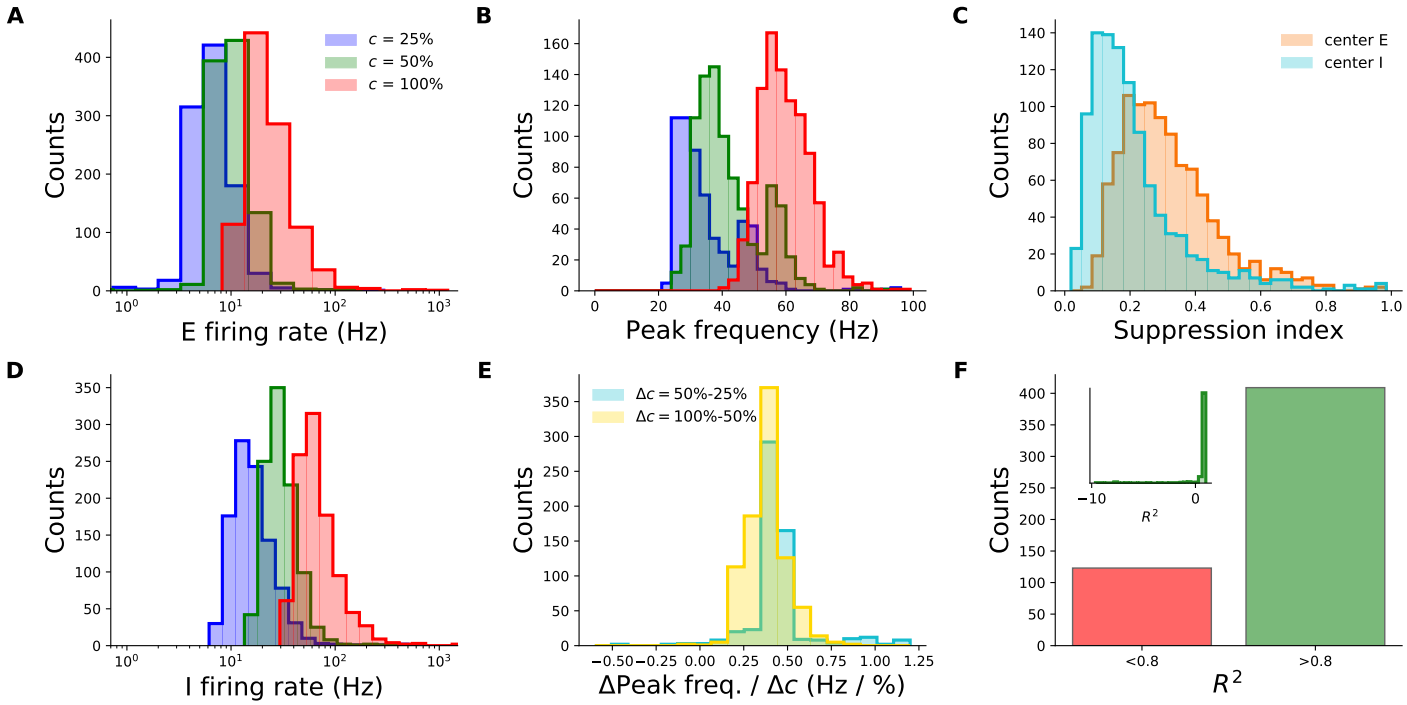

Figure 5. Robustness of the retinotopic SSN to parameter perturbations. We simulated 1000 different retinotopic SSN networks with parameters randomly and independently perturbed up to 10% of their value in the network of Fig. 4. All histograms show counts of these sampled networks. For gamma-related histograms only the fraction of sampled networks exhibiting a gamma peak in the relevant stimulus conditions are included. **A & D:** Distributions of the center *E* and *I* unit's firing rate (logarithmic scale) in response to uniform gratings with contrasts 25% (blue), 50 % (green), and 100% (red). **B:** Distributions of gamma peak frequency at stimulus center, for different contrasts of the largest uniform grating (same color code as in **A**). (The histograms for 25%, 50%, and 100% contrasts include 57.5%, 88%, and 99.8% of sampled networks, respectively.) **C:** Distributions of the suppression index for the center *E* (orange) and *I* (cyan) sub-populations. **E:** Distributions of the change in gamma peak-frequency normalized by the change in stimulus contrast, changing from 25% to 50% (cyan) or from 50% to 100% (yellow). The histograms include 57.5% and 88% of the sampled networks, respectively. The vast majority of perturbed networks produce positive changes in peak frequency as the stimulus contrast grows. **F: H:** The distribution of the goodness-of-fit, as measured by R^2, of the local prediction for gamma peak frequency (the gray line in Fig. 4G, but computed independently for different sampled networks). The goodness-of-fit, R^2, of the gray line in (Fig. 4G) computed for many different simulations. The contrast dependence of gamma peak frequency of the excitatory center sub-population robustly predicts ($R^2 > 0.9$) the peak frequency found in the spatially extended excitatory sub-populations when presenting a Gabor stimulus to the network (green bar). There were fewer where the contrast contrast dependence of the center *E* sub-population did not predict ($R^2 > 0.9$) the locality of contrast dependence (red bar). **Inset:** The full distribution of R^2. 57.3% of networks shown.

networks in a wide, biologically-plausible range of this model's parameter space (see Methods for details).

The sampled networks robustly exhibited surround suppression which was strong in a large fraction of these networks, especially in excitatory neurons (Fig. 6F). Many of these networks, however, failed to produce LFP power-spectrum peaks in the gamma band, or had gamma peak frequencies which decreased, rather than increase, with increasing contrast (Fig. 6H). Figure 6A-C show the LFP power-spectra and size tuning curves for one example network that did show both a robust surround suppression of firing rates as well as gamma peaks that moved to higher frequencies with increasing contrast of a flat grating. However, when presented with the Gabor stimulus, we found that the contrast dependence of gamma peak frequency in this network was far from local, and the peak frequency was shared across most of the retinotopic region stimulted by the Gabor stimulus Fig. 6C-D.

The R^2 of the fit between the actual peak frequency and their local predictions was 0.41 in this case. In none of our sampled networks was the R^2 above 0.5 (see the R^2 histogram in Fig. 6G, and the scatter plot R^2 and suppression index of E rates in Fig. 6I, based on networks that did show gamma peaks at relevant stimulus conditions). We concluded that this model class cannot robustly exhibit both the surround suppression of firing rates and local contrast dependence of gamma peak frequency.

Discussion

In this work we have shown that the expanded SSN is able to robustly display the contrast dependence of gamma peak frequency in both a two-population and a retinotopic network. The retinotopic model successfully balances the trade-off in horizontal connection strength such that both the local contrast dependence of the gamma peak frequency and the surround suppression of firing rates are observed robustly. In order to capture gamma oscillations using the SSN, we expanded the model beyond an E-I network to a varied synaptic network model. Crucially, the SSN account sheds light on the mechanism underlying the contrast dependence of gamma peak frequency and points to the key role of the non-saturating and expansive neural transfer function, observed empirically (Finn et al., 2007; Priebe and Ferster, 2005), in giving rise to this effect.

There exists a class of network models with gamma frequency tied to the single neuronal spiking (Börgers and Kopell, 2003; Traub et al., 1997; Whittington et al., 2011). These models come in two types: those that rely on recurrent connections between inhibitory neurons, known as inhibitory network gamma (ING), and those that rely on recurrent interactions between pyramidal (excitatory) and inhibitory neurons, known as pyramidal-inhibitory network gamma (PING). However, in these ING and PING models generally gamma rhythms emerge from the synchronized regular spiking of different neurons firing at the same frequency across the network. In the visual cortex (as well as other cortical areas), by contrast, neurons have a wide, smooth distribution of firing rates (Buzsáki and Mizuseki, 2014), and typically spike irregularly, in a Poisson-like manner (El Boustani et al., 2007). Lastly these models produce very sharp gamma peaks with higher harmonics (Traub et al., 1997), in contrast to the broad gamma peaks seen in cortical recordings. By contrast, the model we develop here belongs to the class of mean-field or firing rate models (with excitatory and inhibitory neural populations), appropriate for the asychronous and irregular regime of cortical activity (Brunel and Wang, 2003; Kang et al., 2010; Tsodyks et al., 1997).

By using linear response theory to find analytical expressions for the power-spectra, we gained insight into how the SSN accounts for the contrast dependence of gamma frequency. The linear approximation, relates the gamma frequency to the eigenvalues of the linearized system, and in turn relates those to the effective connectivity of the system which is modulated by the neural gains. Due to the specific supralinear neural I/O function of the SSN, these gains increase as activity levels in the network grow, which generically does happen with increasing contrast.

In this work, for simplicity, we assumed an instantaneous I/O function between net synaptic input ($\sum_\beta \mathbf{h}_\beta$) and the output rate. This is based on the approximations discussed in (Fourcaud and Brunel, 2002), which is valid when the fast synaptic filtering time-constants (τ_{AMPA} and τ_{GABA}) are much smaller than the neuronal membrane time-constants. Note that our framework, however, can easily be generalized beyond this approximation by using the full neuronal linear response filter obtained from the Fokker-Planck treatment of (Fourcaud and Brunel, 2002). This biggest impact caused by this treatment would be to render the gains used here frequency dependent (*i.e.* $\Phi \rightarrow \Phi(f)$). We expect this dependence to be weak because we are in the regime of fast synaptic filtering as compared to the neuronal membrane time constant, and so we expect the transfer function to be approximately instantaneous. Therefore we do not expect that including the full neuronal linear response filter would change our qualitative results.

As we have shown, the SSN produces the local contrast dependence of gamma peak frequency and the surround suppression by balancing long-range and local horizontal connections. The local component of the connections used represents some elevated strength within a (micro)column relative to the long-range connections. This predicts that there exists an elevated probability of connection within a (micro)column in the structure of horizontal connectivity in macaque V1. Indeed, it has been noted that anatomical findings on the spatial profile of horizontal connections in the macaque cortex point to such a mixture of short-range or local and long-range connections, with the local component not extending be-

yond 0.4 mm (the size of our modelffs columns) (Voges et al., 2010).

Rodents, however, have a very different V1 organization than macaques. Typically rodents are thought to not have strong columnar organization across the cortex, based mainly on the salt-and-pepper organization of orientation preference in their V1 (Kaschube, 2014). More recently, experimental evidence from mouse V1 suggests that there is no elevated strength in local connections relative to long-range connections (Rossi et al., 2019). As such, we predict that an experiment to (Ray and Maunsell, 2010) but in mouse V1 would find that there is no local contrast dependence of gamma peak frequency, unlike what is observed in macaque.

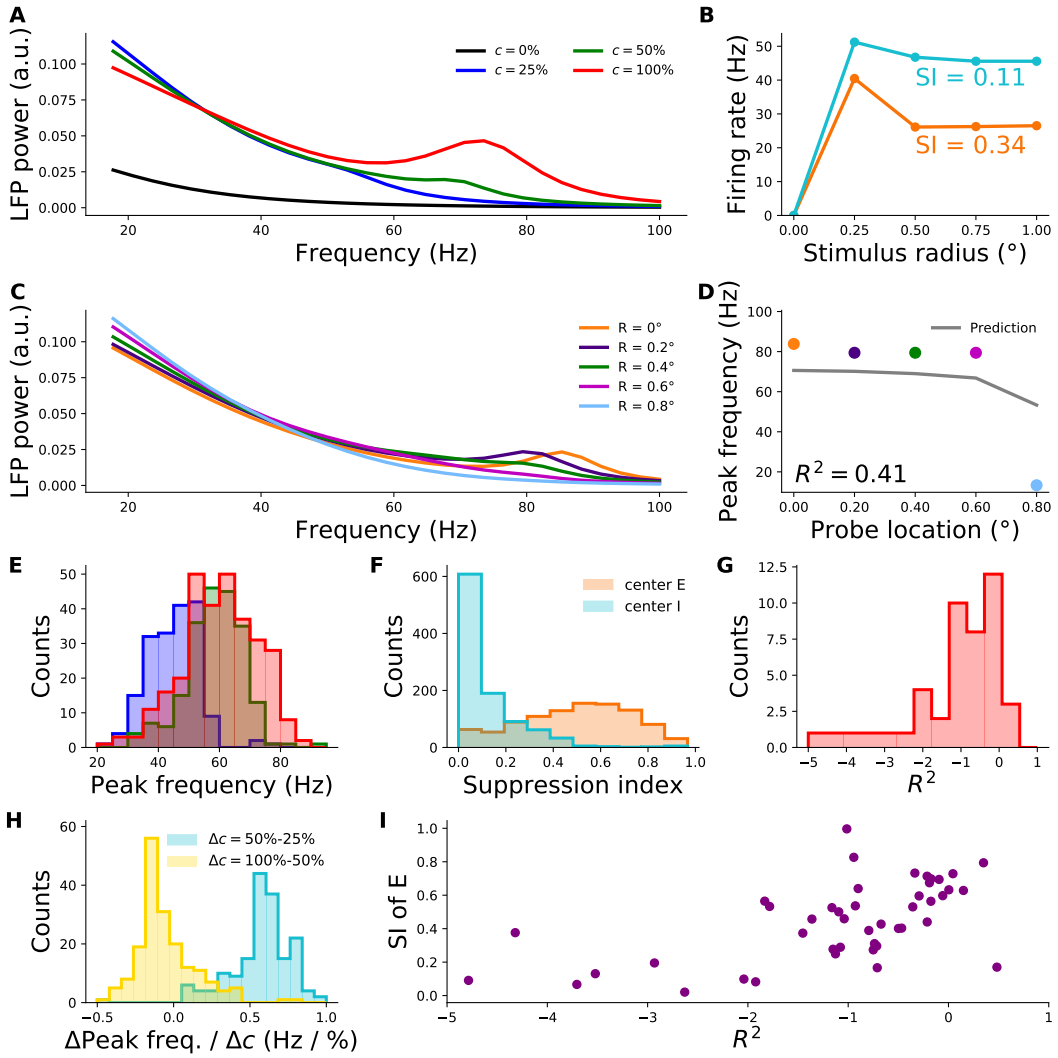

Figure 6. Retinotopic SSN without an excess in intra-columnar *E*-connections fails to capture the local contrast dependence of gamma peak frequency. We simulated a thousand such retinotopic SSN's with randomly sampled parameter-sets. Panels **A-D** show the behavior in the best sampled network in terms of gamma contrast dependence ("example network"). The histogram in panel F includes all sampled networks, while histograms in **E** and **G-I** contain only the minority of sampled networks which exhibited a gamma peak in the relevant stimulus conditions. **A:** LFP power-spectra at the center cortical column in the example network, for different contrasts of the uniform grating stimulus: 0% (black), 25% (blue), 50% (green), 100% (red). **B:** Firing rate size-tuning curves of the center *E* (orange) and *I* (cyan) sub-populations in the example network, based on responses to 100% contrast gratings. **C:** LFP power-spectra in the Gabor stimulus condition at different retinotopic distances from the stimulus center: 0° (orange), 0.2° (navy), 0.4° (green), 0.6° (magenta), and 0.8° (sky blue). **D:** Gamma peak frequency as a function of distance from Gabor stimulus center, for power-spectra in **C**. The gray curve shows the local prediction of the peak frequency given the local contrast in the Gabor stimulus, and the relationship (derived from the power-spectra in **A**) between peak frequency at the center of the uniform grating and its contrast. **E:** Distributions of gamma peak frequency at stimulus center, for different uniform grating contrasts (same color code as in **A**). **F:** Distributions of the suppression index for the center *E* (orange) and *I* (cyan) sub-populations, extracted from size-tuning curves (as in **B**). **G:** Distributions of the change in gamma peak-frequency normalized by the change in stimulus contrast, from 25% to 50% (cyan) or from 50% to 100% (yellow); the respective histograms include 17.3% and 18.2% of sampled networks. **H:** The distribution of the goodness-of-fit, as measured by R^2, of the local prediction for gamma peak frequency (the gray line in **F**, but computed independently for different sampled networks). **I:** The joint distribution of the suppression index of the center *E* population and the locality of gamma contrast dependence (as measured by the R^2 histogrammed in **H**). 4.5% of sampled networks are shown. No sampled network achieved an R^2 above 0.5.

Methods

Stabilized supralinear network (SSN) with different synaptic receptor types

In its original form, the Stabilized Supralinear Network (SSN) is a firing rate network of excitatory and inhibitory neurons that have a supralinear rectified power-law input/output (I/O) transfer function:

$$f(h) = k[h]_+^n \tag{11}$$

where $n > 1$ and $[h]_+ \equiv \max(0, h)$ denotes rectification of h. The dynamics can either be formulated in terms of the inputs to the units (Hennequin et al., 2018) or in terms of their output firing rates (Ahmadian et al., 2013a; Rubin et al., 2015). Here we adopt the former case for which the dynamical state of the network, in a network of N neurons, is given by the N-dimensional vector of inputs vv_t, which evolves according to the dynamical system

$$\mathrm{T}\frac{d\mathbf{h}_t}{dt} + \mathbf{h}_t = Wf(\mathbf{h}_t) + \mathbf{I}_t. \tag{12}$$

Here, $\mathbf{I}$ is the external input vector, $\mathrm{T} = \mathrm{diag}(\tau_1, \ldots, \tau_N)$ is the diagonal matrix of synaptic time constants, and f acts element-wise. Finally, W is the $N \times N$ matrix of recurrent connection weights between the units in the network. This connectivty matrix observes Dale's law, meaning the sign of the weight does not change over columns. If we order neurons such that excitatory neurons appear first and inhibitory neurons second, this matrix takes the form

$$W = \begin{pmatrix} W_{EE} & -W_{EI} \\ W_{IE} & -W_{II} \end{pmatrix} \tag{13}$$

where W_{XY} ($X, Y \in [E, I]$) have non-negative elements.

The above model does not take into account the distinct dynamics of currents through different synaptic receptor channels: AMPA, $\mathrm{GABA_A}$ (henceforth GABA), and NMDA. Only the fast receptors, AMPA and GABA, have timescales relevant to gamma band oscillations. These receptors have very fast rise times, which correspond to frequencies much higher than the gamma band. We therefore ignored the rise times of all receptors. With this assumption, upon arrival of an action potential in a pre-synaptic terminal at time $t = 0$, the post-synaptic current through receptor channel α ($\alpha \in \{\mathrm{A} = \mathrm{AMPA}, \mathrm{G} = \mathrm{GABA}, \mathrm{N} = \mathrm{NMDA}\}$) with decay time τ_α is given by $w\frac{\theta(t)}{\tau_\alpha}e^{-t/\tau_\alpha}$ where $\theta(t)$ is the Heaviside step function and w_α is the contribution of receptor α to the synaptic weight. This is the impulse response solution to the differential equation $\tau_\alpha \frac{dh_\alpha}{dt} + h_\alpha = w\delta(t)$, where $\delta(t)$ is the Dirac delta representing the spike at time $t = 0$. In the mean-field firing rate treatment, the delta function is averaged and is replaced by a smooth rate function $r(t)$. Extending this to cover post-synaptic currents from all synapses into all neurons we obtain the equation

$$\tau_\alpha \frac{d\mathbf{h}_t^\alpha}{dt} + \mathbf{h}_t^\alpha = W^\alpha \mathbf{r}_t \tag{14}$$

where $\mathbf{r}_t$ and $\mathbf{h}^\alpha$ are N-dimensional vectors of the neurons' firings rates and input currents of type α, respectively, and W^α are $N \times N$ matrices containing the contribution of receptor type α to the recurrent synaptic weights. If we add an external input to the right side (before filtering by the synaptic receptors), we obtain Eq. (1). Since AMPA and NMDA only contribute to excitatory synapses, and GABA only to inhibitory ones, in general the W^α have the following block structure

$$W^{\mathrm{A}} = \begin{pmatrix} W_{EE}^{\mathrm{A}} & 0 \\ W_{IE}^{\mathrm{A}} & 0 \end{pmatrix}, \quad W^{\mathrm{N}} = \begin{pmatrix} W_{EE}^{\mathrm{N}} & 0 \\ W_{IE}^{\mathrm{N}} & 0 \end{pmatrix},$$
$$W^{\mathrm{G}} = \begin{pmatrix} 0 & -W_{EI}^{\mathrm{G}} \\ 0 & -W_{II}^{\mathrm{G}} \end{pmatrix}. \tag{15}$$

For simplicity, we further assumed that the fraction of NMDA and AMPA is the same in all excitatory synapses. In this case all W^α can be written in terms of the four blocks of the full connectivity matrix $W \equiv \sum_\alpha W^\alpha$, introduced in Eq. (13):

$$W^{\mathrm{N}} = \frac{\rho_{\mathrm{N}}}{1-\rho_{\mathrm{N}}} W^{\mathrm{A}} = \rho_{\mathrm{N}} \begin{pmatrix} W_{EE} & 0 \\ W_{IE} & 0 \end{pmatrix},$$
$$W^{\mathrm{G}} = \begin{pmatrix} 0 & -W_{EI} \\ 0 & -W_{II} \end{pmatrix}. \tag{16}$$

where the scalar ρ_{N} is the fractional contribution of NMDA to excitatory synaptic weights.

As noted in Results, to close the system of equations for the dynamical variables $\mathbf{h}_t^\alpha$, we have to relate the output rate of a neuron to its total input current, $\mathbf{h}_t^{\mathrm{total}} = \sum_\beta \mathbf{h}_t^\beta$. In general, the relationship between the total input and the firing rate of a neuron, or the mean firing rate of a population of statistically equivalent neurons, is nonlinear and dynamical, meaning the rate at a given instant depends on the preceding history of input, and not just on the instantaneous input. However, as shown by (Brunel et al., 2001; Fourcaud and Brunel, 2002), the firing rate of spiking neurons receiving low-pass filtered noise with fast auto-correlation timescales is approximately a function of the instantaneous input. The fast filtered noise

is exactly what irregular spiking of the spiking network generates after synaptic filtering (as in Eq. (14)) by the fast AMPA and GABA receptors. (While our rate model does not explicitly model (irregular) spiking, it can be thought of as a mean-field approximation to a spiking network where each SSN unit or "neuron" represents a sub-population of spiking neurons, with the rate of that unit representing the average firing rate of the underlying spiking population.) We thus use this static approximation to the I/O transfer function and assume the firing rates of our model units are given by Eq. (2): $\mathbf{r}_t = f(\mathbf{h}_t^{\text{total}}) = f\left(\sum_\beta \mathbf{h}_t^\beta\right)$, where $f(.)$ is the rectified power-law function of Eq. (11).

We do note, however, that this static approximation can be lifted in a straightforward manner at the level of our linearized approximation (which underlies our qualitative understanding of the contrast-dependence of the gamma peak): upon linearization, a dynamic neural transfer function would result in the neural gain variables (see Eq. (21)) becoming frequency-dependent gain *filters*. However, as long as those gain filters are feature-less over the gamma band, their frequency dependence would not qualitatively affect the location of the gamma peak and its stimulus dependence. Thus we expect that the static I/O approximation will not alter our qualitative results.

Modelling of gamma oscillations and local field potential

As discussed in the introduction and Results, gamma oscillations are most consistent with noise-driven damped oscillations. We thus assumed the external input consisted of a time-independent term representing the feed-forward drive due to a static stimulus, and dynamical noise:

$$\mathbf{I}_t^\alpha = \mathbf{I}_{DC}^\alpha + \boldsymbol{\eta}_t^\alpha. \tag{17}$$

Given that external inputs to cortex are excitatory and only fast noise is relevant to gamma oscillations we assumed that $\boldsymbol{\eta}_t^\alpha$ was only nonzero for α =AMPA. We took $\boldsymbol{\eta}_t$ to have independent and identically distributed components (with zero mean) across our sub-population units, and took it to be temporally pink noise, with fast correlation time, τ_{corr}:

$$\langle \eta_i(t_1)\, \eta_j(t_2)\rangle = \delta_{ij}\sigma_\eta^2 e^{-\frac{|t_1-t_2|}{\tau_{\text{corr}}}}. \tag{18}$$

We assume that local field potential (LFP) recordings predominantly measure the inputs to the surrounding pyramidal neurons (Einevoll et al., 2013), and thus in our model use the current input into our excitatory units as the surrogate for LFP. More precisely we take the LFP signal at location $\mathbf{x}$ to be the total current input, $\mathbf{h}^{\text{total}}$, averaged over the E neurons within a given distance of $\mathbf{x}$ (the average could be weighted with weights that decrease with distance). This can be written as the inner product of $\mathbf{h}^{\text{total}}$ with an $\mathbf{x}$-dependent weight vector:

$$LFP_t(\mathbf{x}) \propto \mathbf{e}_\mathbf{x} \cdot \mathbf{h}^{\text{total}} = \sum_\alpha \mathbf{e}_\mathbf{x} \cdot \mathbf{h}^\alpha, \tag{19}$$

where the weight vector $\mathbf{e}_\mathbf{x}$ only has nonzero components for E neurons that are within a given radius of location $\mathbf{x}$. In particular, in the two-population model which lacks retinotopy $\mathbf{e}_\mathbf{x} \equiv \mathbf{e} = (1,0)^{\mathsf{T}}$. In the retinotopic model, we assumed that the spatial range of the LFP recording does not exceed the half-width of our the model's cortical columns (0.2 mm), and therefore we took $\mathbf{e}_\mathbf{x}$ to be a one-hot vector with the component for the E unit at location $\mathbf{x}$ equal to one, and the rest zero.

LFP power-spectra in the linearized approximation

In order to study the power-spectra, and gain intuition about them, we linearized the dynamics around the noise-free fixed point. (Recall that we are modelling gamma as noise-driven damped oscillations, *i.e.* the network is in a regime where without noise it reaches a stable fixed point.) As shown in Results, the fixed point satisfies Eq. (3). The linear approximation consists of a first-order Taylor expansion in powers of the noise, $\boldsymbol{\eta}_t^\alpha$, and noise-driven fluctuations, $\delta\mathbf{h}_t^\alpha \equiv \mathbf{h}_t^\alpha - \mathbf{h}_*^\alpha$, around the stable fixed point. (Note that while the fixed point equation only involves the total current $\mathbf{h}_* \equiv \sum_\alpha \mathbf{h}_*^\alpha$, after numerically finding $\mathbf{h}_*$, we can obtain the fixed-point value of the receptor-specific currents via $\mathbf{h}_*^\alpha = W^\alpha f(\mathbf{h}_*) + I_{DC}^\alpha$.) This yields

$$\tau^\alpha \frac{d\delta\mathbf{h}_t^\alpha}{dt} = -\delta\mathbf{h}^\alpha + W^\alpha \Phi \sum_\beta \delta\mathbf{h}_t^\beta + \boldsymbol{\eta}_t, \tag{20}$$

where we defined the gain matrix Φ as a diagonal matrix whose diagonal entries are

$$\Phi_{ii} \equiv f'(h_{i*}) = nk[h_{i*}]_+^{n-1} = nk^{\frac{1}{n}}\mathbf{r}_{i*}^{1-\frac{1}{n}}. \tag{21}$$

Taking the Fourier transform of (20), and solving for $\delta\widetilde{\mathbf{h}}_f^\alpha$ (the Fourier transform of $\delta\mathbf{h}_t^\alpha$, where f denotes frequency) we obtain

$$\delta\widetilde{\mathbf{h}}_f^\alpha = \sum_\beta G^{\alpha\beta}(f)\,\widetilde{\boldsymbol{\eta}}_f^\beta, \tag{22}$$

where the Green's function, $G_h^{\alpha\beta}(f)$, is given by

$$G^{\alpha\beta}(f) \equiv \sum_\beta [(-i2\pi f\tau^\alpha + 1)\delta_{\alpha\beta} - W^\alpha\Phi]^{-1}. \tag{23}$$

Since, by Eq. (19), the LFP is a linear function of $\mathbf{h}^\alpha$, the power-spectrum of LFP can be written in terms of the cross-spectrum matrix of $\delta\tilde{\mathbf{h}}_f^\alpha$, which we denote by $C_h^{\alpha,\beta}(f)$. Specifically

$$P_{\text{LFP}}(f) = \sum_{\alpha,\beta} \mathbf{e}_\mathbf{x}^\mathsf{T}\, C_h^{\alpha,\beta}(f)\,\mathbf{e}_\mathbf{x}. \tag{24}$$

Using Eq. (22) and $C_h^{\alpha,\beta}(f) \propto \langle \delta\tilde{\mathbf{h}}_f^\alpha \delta\tilde{\mathbf{h}}_f^{\beta\dagger}\rangle$ we have

$$\begin{aligned} C_h^{\alpha,\beta}(f) &= \sum_{\gamma,\delta} G^{\alpha,\gamma}(f)\, C_\eta^{\gamma,\delta}(f)\, G^{\delta,\beta}(f)^\dagger, \\ &= G^{\alpha,\mathrm{A}}(f)\, C_\eta^{\mathrm{A},\mathrm{A}}(f)\, G^{\mathrm{A},\beta}(f)^\dagger. \end{aligned} \tag{25}$$

Here, $C_\eta^{\gamma,\epsilon}(f)$ is the cross-spectrum of the input noise, and in the second line we relied on our assumption that noise only enters the AMPA channel, and thus only $\gamma = \delta = \mathrm{A} \equiv$ AMPA contribute to the sums. From Eq. (18), we have $C_\eta^{\mathrm{A},\mathrm{A}}(f) = P_\eta(f)\,\mathbf{I}_{N\times N}$, where

$$P_\eta(f) = \frac{2\tau_{\text{corr}}\sigma_\eta^2}{|1 - 2\pi i\tau_{\text{corr}} f|^2} \tag{26}$$

is the power-spectrum of noise. We finally obtain

$$\begin{aligned} P_{\text{LFP}}(f) &= P_\eta(f)\,\|\mathbf{u}_\mathbf{x}(f)\|^2, \\ \mathbf{u}_\mathbf{x}(f) &\equiv \sum_\beta G^{\beta,\mathrm{A}}(f)^\dagger \mathbf{e}_\mathbf{x}. \end{aligned} \tag{27}$$

Definition of gamma peak frequency and width

As in Ray and Maunsell 2010, we identified the gamma peak frequency with the frequency (within the gamma band, 30-100 Hz) at which the difference of the evoked ($c > 0$) and spontaneous ($c = 0$) LFP log-spectra (or the ratio of those spectra) is maximized:

$$f_{\max} = \text{argmax}\left[\log P_{\text{LFP}}(f)|_{c>0} - \log P_{\text{LFP}}(f)|_{c=0}\right]. \tag{28}$$

As a measure of gamma half-width, we used the half-width at half-height of the ratio $\frac{P_{\text{LFP}}(f)|_{c>0}}{P_{\text{LFP}}(f)|_{c=0}}$.

Parametrization of the two-population and retinotopic models

The 2x2 (full) connectivity matrix of the 2-population model is parametrized by the four parameters J_{ab} ($a, b \in \{E, I\}$) as follows:

$$W = \begin{pmatrix} J_{EE} & -J_{EI} \\ J_{IE} & -J_{II} \end{pmatrix}. \tag{29}$$

The DC stimulus input corresponds to feedforward excitatory inputs from LGN and targets both sub-populations only via the AMPA channel (since this input is time-independent, its distribution across NMDA and AMPA channels is actually of no consequence). As in the original SSN, we assumed this input scales linearly with contrast, c, but with varying relative strengths to the E and I captured by the two parameters g_E and g_I:

$$\mathbf{I}_{DC} = c\begin{pmatrix} g_E \\ g_I \end{pmatrix}. \tag{30}$$

In the retinotopic model we index the neurons by their E/I type and retinotopic location. We parametrized the recurrent connection weight from the pre-synaptic E and I units at location $\mathbf{y}$ to the type a ($a \in [E, I]$) post-synaptic unit at location $\mathbf{x}$ by

$$W_{\mathbf{x},a|\mathbf{y},E} \propto J_{a,E}\left[\lambda_{a,E}\,\delta_{\mathbf{x},\mathbf{y}} + (1 - \lambda_{a,E})e^{-\frac{\|\mathbf{x}-\mathbf{y}\|}{\sigma_{a,E}}}\right] \tag{31}$$

for excitatory projections, and

$$W_{\mathbf{x},a|\mathbf{y},I} \propto J_{a,I}\, e^{-\frac{(\mathbf{x}-\mathbf{y})^2}{2\sigma_{a,I}^2}}, \tag{32}$$

for inhibitory ones. We are using proportionality instead of equal signs in the above equations, because a normalization was done such that the total weight of each type received by a unit was given by the corresponding J_{ab} (independent of the σ_{ab} and λ_{ab} parameters). Recurrent connectivity was thus parametrized by the 2x2 matrices J_{ab} and σ_{ab}, the two $\lambda_{a,E}$, and the NMDA fraction, ρ_N. For σ_{II} and σ_{EI} we used values (see Table 1) small compared to the distance between neighboring columns (0.4 mm) so that inhibition was effectively local (*i.e.*, intra-columnar).

We modeled the external stimulus input to the type a unit at $\mathbf{x}$ by

$$I^{DC}_{a,\mathbf{x}} = c\, g_a\, I_{\mathbf{x}} \qquad (a \in \{E, I\}). \tag{33}$$

For a grating of radius r_{grat} we modeled the spatial contrast profile, $I_{\mathbf{x}}$, as

$$I_{\mathbf{x}} = \frac{1}{1 + e^{\frac{\|\mathbf{x}\| - r_{\text{grat}}}{w_{\text{RF}}}}}. \tag{34}$$

The parameter w_{RF} smooths the edges of the grating (due to feedforward filtering by receptive fields of width $\sim w_{\text{RF}}$). Note that for $r_{\text{grat}} \gg w_{\text{RF}}$ (which was true for most grating sizes employed), local contrast is nearly uniform under the support of the external input (except within a "boundary layer" of width w_{RF} near $\|x\| = r_{\text{grat}}$). For the Gabor stimulus we have

$$I_{\mathbf{x}} = e^{-\frac{\|\mathbf{x}\|^2}{2\sigma^2_{\text{Gabor}}}}. \tag{35}$$

We took $\sigma_{Gabor} = 0.5°$, as in Ray and Maunsell 2010, and the peak contrast (c in Eq. (33)) was always 100% for this stimulus.

Explorations of model parameter space

See Table 1 below for the values of all parameters or parameter ranges for models used in different figures. For the models used in Figs. 1 and 4, we found their figure-specific parameters (J_{ab} and g_a which are shared in both figures, and $\sigma_{a,E}$ and $\lambda_{a,E}$ for Fig. 4) using random sampling (we sampled these parameters uniformly and independently within biologically plausible ranges) searching for networks that would exhibit the local contrast-dependence of the gamma peak together with strong surround suppression.

For studying the robustness of the contrast dependence of gamma frequency in the two-population model in Fig. 2, and in the case of the retinotopic SSN with a smooth fall-off of excitatory horizontal connectivity in Fig. 6, we sampled parameters from wide biologically plausible ranges. To determine these ranges for the recurrent and feedforward weights, we first made rough biological point estimates for the recurrent E and I weights (*i.e.*, J_{aE} and J_{aI}, respectively, for $a \in \{E, I\}$), as well as the (excitatory) feedforward weights (g_E and g_I); we denote this estimates by J^*_E, J^*_I and g^*, respectively. We then independently varied parameters controlling each type of weight between 0.5 to 1.5 times those estimates (see Table 1 for the actual values). Finally, we assumed that recurrent V1 excitatory synapses are dominated by AMPA, rather than NMDA, and therefore sampled ρ_N uniformly at random in the interval $[0, 0.5]$.

To estimate the mid-range estimates, J^*_E, J^*_I and g^*, we relied on empirical estimates of the effect of recurrent and feedforward inputs on the membrane voltage of a post-synaptic neuron. Note that while J_{ab} (and thus J^*_E and J^*_I), have dimensions of voltage (such that the recurrent input $W\mathbf{r}$ has our units of current), g_a (and thus g^*) have dimensions of current. In our model, we measured the currents in units of mV/s, by including an implicit factor of membrane capacitance in them. The membrane potential response to a unit current is normally given by the membrane resistance, which in our units becomes the membrane time constant, which we take to be $\tau_m = 0.01$ s. So to obtain an estimate of g^* from voltage measurements, we need to multiply the estimate by $\tau_m^{-1} = 100\ \text{s}^{-1}$.

We estimated the effect of feedforward inputs on membrane voltage using measurements in cats and mice (Chung and Ferster, 1997, 1998; Ferster et al., 1996; Finn et al., 2007; Li et al., 2013; Lien and Scanziani, 2013) (see Ahmadian and Miller 2021 for a review and discussion of these measurements). Based on these measurements, we estimate the maximum feedforward input, achieved for 100% contrast to be on the order of the rest to threshold distance, which is around 20 mV (Constantinople and Bruno, 2013). This yields $g^* \sim \tau_m^{-1} 20\,\text{mV}/(100\%) = 20$ mV/s per 1% contrast. The J_{ab} parameters measure the total synaptic weight, which biologically is given by a unitary excitatory or inhibitory (depending on b) post-synaptic potential (EPSP or IPSP) times the total number of pre-synaptic V1 neurons, K_b, of type b. Based on anatomical measurements for sensory cortex (reviewed in Ahmadian and Miller 2021) we estimate the effective K_E to be ~ 400 (with a wide margin of uncertainty). And based on electrophysiological measurements we assume the median EPSP amplitude to be ~ 0.5 mV. This yields $J^*_E = 0.5 \times 400 = 200$ mV. For unitary IPSP amplitude, we used the same value of 0.5 mV, but assumed half as many inhibitory pre-synaptic inputs, due to the smaller number of inhibitory cells in the circuit. We thus took $J^*_I = J^*_E/2$.

In Fig. 6, studying the retinotopic SSN with a smooth fall-off of excitatory horizontal connectivity (*i.e.*, with $\lambda_{EE} = \lambda_{IE} = 0$), in addition to random sampling of J_{ab} and g_a from the above ranges, we also sampled the length-scales

Parameter	Fig. 1	Figs. 2-3	Fig. 4	Fig. 5	Fig. 6	Unit	Description
n	2					-	power-law I/O exponent
k	2×10^{-5}					$mV^{-n} \cdot s$	power-law I/O pre-factor
τ_{corr}	5					ms	noise correlation time
τ_{AMPA}	5					ms	AMPA decay time
τ_{GABA}	7					ms	$GABA_A$ decay time
τ_{NMDA}	100					ms	NMDA decay time
ρ_N	0.5	0 - 0.5	0.5	*	0.5 †	-	NMDA share of excitation
J_{EE}	198	100 - 300	198	*	188 †	mV	total E $\rightarrow$ E connection weight
J_{IE}	225	100 - 300	225	*	161 †	mV	total E $\rightarrow$ I connection weight
J_{EI}	73.8	50 - 150	73.8	*	141 †	mV	total I $\rightarrow$ E connection weight
J_{II}	55.5	50 - 150	55.5	*	83.2 †	mV	total I $\rightarrow$ I connection weight
g_E	16.5	10 - 30	16.5	*	25.9 †	mV/s	*E* feedforward current per 1% contrast
g_I	11.6	5 - 15	11.6	*	10.3 †	mV/s	*I* feedforward current per 1% contrast
λ_{EE}	-	-	0.4	*	0	-	locality of E $\rightarrow$ E connections
λ_{IE}	-	-	0.7	*	0	-	locality of E $\rightarrow$ E connections
σ_{EE}	-	-	0.2	*	0.22 †	mm	range of E $\rightarrow$ E connections
σ_{IE}	-	-	0.4	*	0.24 †	mm	range of E $\rightarrow$ E connections
σ_{EI}	-	-	0.09			mm	range of E $\rightarrow$ E connections
σ_{II}	-	-	0.09			mm	range of E $\rightarrow$ E connections
N_{col}	1	1	17^2			-	number of cortical columns
L	-	-	6.4			mm	retinotopic network width
Δx	-	-	0.4			mm	cortical column width
M	-	-	2			mm/degrees	cortical magnification factor
w_{RF}	-	-	0.04°			degrees	grating input's margin width
σ_{Gabor}	-	-	0.5°			degrees	Gabor stimulus sigma

Table 1. Parameters of models used in different figures. Parameter values indicated by * in the column for Fig. 5 were sampled uniformly between 0.9 to 1.1 times their value in Fig. 4. †: the parameters given for Fig. 6 are for the example network of panels A-D; in panels E-I, the J_{ab}, g_a, and ρ_N parameters were sampled from the same ranges as in Figs. 2-3, while σ_{aE} parameters were sampled from the range 0.15 mm - 0.55 mm, uniformly and independently, subject to $\sigma_{IE} > \sigma_{EE}$.

of excitatory horizontal connections from a biologically plausible range: $\sigma_{EE}, \sigma_{IE} \in [0.15, 0.5]$ mm. We sampled these randomly and uniformly from the above range, subject to the condition $\sigma_{I,E} > \sigma_{E,E}$, which is necessary for obtaining surround suppression (Rubin et al., 2015).

Acknowledgements

We thank Takafumi Arakaki for technical help throughout this research, and Luca Mazzucato for valuable comments on the manuscript. CH would like to acknowledge technical help and invaluable feedback from Gabriel Barello, Elliott Abe and David Wyrick. YA was supported by start-up funds and an Incubating Interdisciplinary Initiatives (I3) Award from the University of Oregon. KDM is supported by NSF DBI-1707398, NIH U01NS108683, NIH R01EY029999, NIH U19NS107613, Simons Foundation award 543017, and the Gatsby Charitable Foundation.

References

Ahmadian, Y. and Miller, K. D. (2021). What is the dynamical regime of cerebral cortex? *Neuron*, 109(21):3373–3391.

Ahmadian, Y., Rubin, D. B., and Miller, K. D. (2013a). Analysis of the stabilized supralinear network. *Neural Computation*, 25(8):1994–2037.

Ahmadian, Y., Rubin, D. B., and Miller, K. D. (2013b). Analysis of the stabilized supralinear network. *Neural Computation*, 25:1994–2037.

Anderson, J., Lampl, I., Gillespie, D., and Ferster, D. (2000). The contribution of noise to contrast invariance of orientation tuning in cat visual cortex. *Science (New York, NY)*, 290(5498):1968–1972.

Barbieri, F., Mazzoni, A., Logothetis, N. K., Panzeri, S., and Brunel, N. (2014). Stimulus dependence of local field potential spectra: Experiment versus theory. *Journal of Neuroscience*, 34(44):14589–14605.

Börgers, C. and Kopell, N. (2003). Synchronization in networks of excitatory and inhibitory neurons with sparse, random connectivity. *Neural Computation*, 15(3):509–538.

Brunel, N., Chance, F. S., Fourcaud, N., and Abbott, L. F. (2001). Effects of synaptic noise and filtering on the frequency response of spiking neurons. *Physical Review Letters*, 86(10):2186–2189.

Brunel, N. and Wang, X.-J. (2003). What determines the frequency of fast network oscillations with irregular neural discharges? i. synaptic dynamics and excitation-inhibition balance. *J Neurophysiol*, 90(1):415–430.

Burns, S. P., Xing, D., and Shapley, R. M. (2011). Is gamma-band activity in the local field potential of v1 cortex a "clock" or filtered noise? *J Neurosci*, 31(26):9658–9664.

Burns, S. P., Xing, D., Shelley, M. J., and Shapley, R. M. (2010). Searching for autocoherence in the cortical network with a time-frequency analysis of the local field potential. *Journal of Neuroscience*, 30(11):4033–4047.

Buzsáki, G. and Chrobak, J. J. (1995). Temporal structure in spatially organized neuronal ensembles: a role for interneuronal networks. *Current Opinion in Neurobiology*, 5(4):504–510.

Buzsáki, G. and Mizuseki, K. (2014). The log-dynamic brain: How skewed distributions affect network operations. *Nature Reviews Neuroscience*, 15(4):264–278.

Buzsáki, G. and Wang, X.-J. (2012). Mechanisms of Gamma Oscillations. *Annual Review of Neuroscience*, 35(1):203–225.

Cavanaugh, J., Bair, W., and Movshon, J. (2002). Nature and interaction of signals from the receptive field center and surround in macaque v1 neurons. *Journal of Neurophysiology*, 88(5):2530–2546.

Chung, S. and Ferster, D. (1997). The size of thalamic input to simple cells of the cat visual cortex. *Soc. Neurosci. Abstr.*, 23:2059.

Chung, S. and Ferster, D. (1998). Strength and orientation tuning of the thalamic input to simple cells revealed by electrically evoked cortical suppression. *Neuron*, 20:1177–89.

Constantinople, C. M. and Bruno, R. M. (2013). Deep cortical layers are activated directly by thalamus. *Science*, 340:1591–1594.

Dayan, P. and Abbott, L. (2001). *Theoretical Neuroscience*. MIT Press, Cambridge.

Draguhn, A. and Buzsáki, G. (2004). Neuronal Oscillations in Cortical Networks. *Science*, 304(June):1926–1930.

Einevoll, G. T., Kayser, C., Logothetis, N. K., and Panzeri, S. (2013). Modelling and analysis of local field potentials for studying the function of cortical circuits. *NATURE REVIEWS NEUROSCIENCE*, 14(11):770–None.

El Boustani, S., Pospischil, M., Rudolph-Lilith, M., and Destexhe, A. (2007). Activated cortical states: Experiments, analyses and models. *Journal of Physiology Paris*, 101(1-3):99–109.

Ferster, D., Chung, S., and Wheat, H. (1996). Orientation selectivity of thalamic input to simple cells of cat visual cortex. *Nature*, 380:249–252.

Finn, I. M., Priebe, N. J., and Ferster, D. (2007). The emergence of contrast-invariant orientation tuning in simple cells of cat visual cortex. *Neuron*, 54(1):137–152.

Fourcaud, N. and Brunel, N. (2002). Dynamics of the firing probability of noisy integrate-and-fire neurons. *Neural Computation*, 14:2057–2110.

Fries, P. (2005). A mechanism for cognitive dynamics: Neuronal communication through neuronal coherence. *Trends in Cognitive Sciences*, 9(10):474–480.

Fries, P. (2015). Rhythms for Cognition: Communication through Coherence. *Neuron*, 88(1):220–235.

Fries, P., Nikolić, D., and Singer, W. (2007). The gamma cycle. *Trends in Neurosciences*, 30(7):309–316.

Gieselmann, M. A. and Thiele, A. (2008). Comparison of spatial integration and surround suppression characteristics in spiking activity and the local field potential in macaque v1. *Eur J Neurosci*, 28(3):447–459.

Gilbert, C. D. and Wiesel, T. N. (1989). Columnar specificity of intrinsic horizontal and corticocortical connections in cat visual cortex. *Journal of Neuroscience*, 9(7):2432–2422.

Hennequin, G., Ahmadian, Y., Rubin, D. B., Lengyel, M., and Miller, K. D. (2018). The Dynamical Regime of Sensory Cortex: Stable Dynamics around a Single Stimulus-Tuned Attractor Account for Patterns of Noise Variability. *Neuron*, 98(4):846–860.e5.

Henrie, J. A. and Shapley, R. (2005). LFP power spectra in V1 cortex: The graded effect of stimulus contrast. *Journal of Neurophysiology*, 94(1):479–490.

Hopfield, J. J. (2004). Encoding for computation: Recognizing brief dynamical patterns by exploiting effects of weak rhythms on action-potential timing. *Proceedings of the National Academy of Sciences of the United States of America*, 101(16):6255–6260.

Jefferys, J. G., Traub, R. D., and Whittington, M. A. (1996). Neuronal networks for induced '40 Hz' rhythms. *Trends in Neurosciences*, 19(5):202–208.

Jia, X., Xing, D., and Kohn, A. (2013). No consistent relationship between gamma power and peak frequency in macaque primary visual cortex. *Journal of Neuroscience*, 33(1):17–25.

Kang, K., Shelley, M., Henrie, J. A., and Shapley, R. (2010). Lfp spectral peaks in v1 cortex: network resonance and cortico-cortical feedback. *J Comput Neurosci*, 29(3):495–507.

Kaschube, M. (2014). Neural maps versus salt-and-pepper organization in visual cortex. *Current Opinion in Neurobiology*, 24(1):95–102.

Ledoux, E. and Brunel, N. (2011). Dynamics of Networks of Excitatory and Inhibitory Neurons in Response to Time-Dependent Inputs. *Frontiers in Computational Neuroscience*, 5:1–17.

Li, L. Y., Li, Y. T., Zhou, M., Tao, H. W., and Zhang, L. I. (2013). Intracortical multiplication of thalamocortical signals in mouse auditory cortex. *Nat. Neurosci.*, 16:1179–1181.

Lien, A. D. and Scanziani, M. (2013). Tuned thalamic excitation is amplified by visual cortical circuits. *Nat. Neurosci.*, 16:1315–1323.

Ni, J., Wunderle, T., Lewis, C. M., Desimone, R., Diester, I., and Fries, P. (2016). Gamma-Rhythmic Gain Modulation. *Neuron*, 92(1):240–251.

Priebe, N. J. and Ferster, D. (2005). Direction selectivity of excitation and inhibition in simple cells of the cat primary visual cortex. *Neuron*, 45:133–45.

Priebe, N. J. and Ferster, D. (2008). Inhibition, spike threshold, and stimulus selectivity in primary visual cortex. *Neuron*, 57(4):482–497.

Ray, S. and Maunsell, J. H. R. (2010). Differences in gamma frequencies across visual cortex restrict their possible use in computation. *Neuron*, 67(5):885–896.

Rossi, L. F., Harris, K., and Carandini, M. (2019). Excitatory and inhibitory intracortical circuits for orientation and direction selectivity. *bioRxiv*, page 556795.

Rubin, D. B. and Miller, K. D. (2010). Normalization in a nonlinear circuit model of V1. *Program No. 126.1. 2010 Neuroscience Meeting Planner. Washington, DC: Society for Neuroscience*, Online.

Rubin, D. B., Van Hooser, S. D., and Miller, K. D. (2015). The stabilized supralinear network: a unifying circuit motif underlying multi-input integration in sensory cortex. *Neuron*, 85(2):402–417.

Schwabe, L., Ichida, J. M., Shushruth, S., Mangapathy, P., and Angelucci, A. (2010). Contrast-dependence of surround suppression in macaque v1: Experimental testing of a recurrent network model. *NeuroImage*, 52(3):777–792.

Singer, W. (1999). Neuronal synchrony: a versatile code for the definition of relations? *Neuron*, 24(1):49–65.

Traub, R. D., Jefferys, J. G. R., and Whittington, M. A. (1997). Simulation of Gamma Rhythms in Networks of Interneurons and Pyramidal Cells. *Journal of Computational Neuroscience*, page 10.

Tsodyks, M. V., Skaggs, W. E., and Sejnowski, T. J.and McNaughton, B. L. (1997). Paradoxical effects of external modulation of inhibitory interneurons. *J. Neurosci.*, 17:4382–4388.

Voges, N., Schüz, A., Aertsen, A., and Rotter, S. (2010). A modeler's view on the spatial structure of intrinsic horizontal connectivity in the neocortex. *Progress in Neurobiology*, 92(3):277–292.

Whittington, M. A., Cunningham, M. O., LeBeau, F. E. N., Racca, C., and Traub, R. D. (2011). Multiple origins of the cortical gamma rhythm. *Developmental Neurobiology*, 71(1):92–106.

Xing, D., Shen, Y., Burns, S., Yeh, C. I., Shapley, R., and Li, W. (2012). Stochastic generation of gamma-band activity in primary visual cortex of awake and anesthetized monkeys. *Journal of Neuroscience*, 32(40):13873–13880.

Appendix 1

Proof that spectrum of a synaptic model with only AMPA and GABA is the same as the spectrum of an E/I rate model

Here we prove that the spectrum of a linearized synaptic model without NMDA is the same as the spectrum of a linearized E/I rate model, with the exchange $\tau_{AMPA} \to \tau_E$ and $\tau_{GABA} \to \tau_I$. This means that, in particular, the formulae of (Tsodyks et al., 1997) for eigenvalues in a 2-neuron/population model still hold for this model with the above replacements.

We start by rewriting the inverse Green's function, using the Green's function defined in Eq. (23), which we now write in full matrix form. We will also start general, allowing for q different receptor types (we also write in terms of the angular frequency $\omega = 2\pi f$).

$$G(\omega)^{-1} = A - \mathbf{W}\Phi P \tag{36}$$

where we define

$$A := -i\omega\mathbf{T} + \mathbb{I} \qquad \in \mathbb{R}^{qN\times qN} \tag{37}$$

$$\mathbf{W} := \begin{pmatrix} W^A \\ W^G \\ W^N \\ \vdots \end{pmatrix} \qquad \in \mathbb{R}^{qN\times N} \tag{38}$$

$$P := \mathbb{I}_{N\times N} \otimes \mathbf{1}_q^{\mathsf{T}} = (\mathbb{I}_{N\times N}, \mathbb{I}_{N\times N}, \mathbb{I}_{N\times N}, \ldots) \qquad \in \mathbb{R}^{N\times qN} \tag{39}$$

where $\mathbf{T} = \mathrm{diag}(\boldsymbol{\tau}_s) \otimes \mathbb{I}_{N\times N}$ and $\boldsymbol{\tau}_s \in \mathbb{R}$ (in our case $\boldsymbol{\tau}_s = (\tau_A, \tau_G, \tau_N)$ or (τ_A, τ_G)), and $\mathbf{1}_q^{\mathsf{T}} = (1, \ldots, 1) \in \mathbb{R}^q$.

The eigenvalue spectrum correspond to values of $z = -i\omega$ which make the determinant of $G(\omega)^{-1}$ vanish. Noting that the second term in Eq. (36) is rank-deficient (has at most rank N, instead of full-rank qN), we make use of the "matrix determinant lemma" to write:

$$\det(G^{-1}(\omega)) = \det(A)\det(\mathbb{I}_{N\times N} - PA^{-1}\mathbf{W}\Phi) \tag{40}$$

It is not hard to see that

$$PA^{-1} = \left(\frac{\mathbb{I}_{N\times N}}{-i\omega\tau_A + 1}, \frac{\mathbb{I}_{N\times N}}{-i\omega\tau_G + 1}, \frac{\mathbb{I}_{N\times N}}{-i\omega\tau_N + 1}, \ldots\right) \tag{41}$$

and therefore

$$PA^{-1}\mathbf{W} = \sum_{\alpha=1}^{q} \frac{1}{-i\omega\tau_\alpha + 1} W^\alpha \tag{42}$$

We now limit to $q = 2$ with only AMPA and GABA.

$$PA^{-1}\mathbf{W} = \frac{1}{-i\omega\tau_A + 1} W^A + \frac{1}{-i\omega\tau_G + 1} W^G = W\widetilde{A}^{-1} \quad (43)$$

where we have made use of the specific forms of W^A and W^G (namely, that they have zero columns for inhibitory and excitatory neurons, respectively) from Eq. (16), and where we have defined

$$W = \sum_\alpha W^\alpha \qquad \in \mathbb{R}^{N\times N} \quad (44)$$

$$\widetilde{A} := z\widetilde{T} + \mathbb{I}_{N\times N} \quad (45)$$

with $\widetilde{T} = \text{diag}(\tilde{\tau}) \in \mathbb{R}^{N\times N}$ where $\tilde{\tau} = (\tau_A, \ldots, \tau_G, \ldots) \in \mathbb{R}^N$ is the N-dimensional vector with first N_E components equal to τ_A and the last N_I components equal to τ_G. After identifying $\tau_{A/G}$ with $\tau_{E/I}$, we thus see that $\widetilde{T}$ is the same as the T matrix of the **r**-model (which is N-dimensional), as is W its connectivity matrix. Also noting that $(z\widetilde{T} + \mathbb{I}_{N\times N})^{-1}$ and Φ are both diagonal, we can commute them in Eq. (43) to obtain:

$$\det(G^{-1}(\omega)) = \det(A)\det(\mathbb{I}_{N\times N} - W\Phi\widetilde{A}^{-1}) \quad (46)$$

$$= \frac{\det(A)}{\det(\widetilde{A})}\det(z\widetilde{T} + \mathbb{I}_{N\times N} - W\Phi) \quad (47)$$

$$= \frac{\det(A)}{\det(\widetilde{A})}\det(z\widetilde{T} + \mathbb{I}_{N\times N} - \Phi W) \quad (48)$$

(to get the last line, do a similarity transform with Φ, of the matrix in the last determinant).

Now it is explicit that the zeros of the last determinant factor are the eigenvalues of the N-dimensional **r**-system (after $\tau_{A/G} \leftrightarrow \tau_{E/I}$ identification).

The first factor, on the other hand, can be written as:

$$\frac{\det(A)}{\det(\tilde{A})} = \frac{(z\tau_A + 1)^N (z\tau_G + 1)^N}{(z\tau_A + 1)^{N_E}(z\tau_G + 1)^{N_I}} = (z\tau_A + 1)^{N_I}(z\tau_G + 1)^{N_E} \quad (49)$$

So the spectrum also has N additional *real* eigenvalues (in addition to those of the **r**-model) with values $-\tau_A^{-1}$ and $-\tau_G^{-1}$, and multiplicities, N_I and N_E, respectively. (Thus in total we have $2N$ eigenvalues as we should.)

In particular, all oscillatory/complex eigenvalues are exactly those of the **r**-model in the no-NMDA case, which in the 2-neuron case are given by the formulae in Tsodyks et al. 1997.

Approximate statement about role of NMDA: We consider two regimes for the effect of NMDA:

1. when $|z|$ or ω are very small compared to the NMDA time-constant: $\omega \ll \tau_N^{-1}$.

2. when $|z|$ or ω are very large compared to the NMDA time-constant: $\omega \gg \tau_N^{-1}$.

The first regime is relevant for DC response and DC properties (such as surround suppression of steady-state rates). The second regime is approximately valid for gamma oscillations, thanks to the relatively high frequency of those.

In regime 1, it is obvious that the breakdown of E weights into the two types doesn't have any effects, simply because (setting ω to 0) time-scales don't play any role here. So the parameter ρ_N makes no difference to fixed point response properties.

In regime 2, looking at Eq. (42), we note that the prefactor $\frac{1}{-i\omega\tau_\alpha+1}$ for NMDA is very small and can be ignored. This means that for high frequencies (*e.g.*, approximately frequencies around gamma) we can simply kill all NMDA weights, and only consider the AMPA weight matrix, W^A. In particular, the model where $W^A \propto W^N$, then the effect of NMDA on the gamma peak is approximately equivalent to reducing total excitatory weights (which all affect DC properties) by a scalar factor (which in our formalism is $1 - \rho_N$) when it comes to gamma properties.

Appendix 2

Theorems for the two-population model

We consider now the case of a two-neuron model with one excitatory and one inhibitory neuron (the neurons in all models of this article should be thought of as "mean field" neurons, each representing a statistically homogenous population of neurons of excitatory or inhibitory type), what we have here called the two-population model. We will also assume no NMDA contribution (or equivalently work in the very slow NMDA regime, and replace all excitatory weights with their AMPA part, as explained at the end of Appendix 1).

In this case the gamma peak frequency is closely approximated by the imaginary part of the eigenvalues of the

Jacobian matrix:

$$\mathcal{J} = -\mathbf{T}^{-1} + \mathbf{T}^{-1}\mathbf{W}\Phi \tag{50}$$

$$= \begin{pmatrix} \gamma_E(-1 + W_{EE}\Phi_E) & -\gamma_E W_{EI}\Phi_I \\ \gamma_I W_{IE}\Phi_E & \gamma_I(-1 - W_{II}\Phi_I) \end{pmatrix} \tag{51}$$

where we defined $\gamma_E \equiv \tau_{AMPA}^{-1}$ and $\gamma_I \equiv \tau_{GABA}^{-1}$. Noting that the trace and determinant of $\mathcal{J}$ yield the sum and product of the eigenvalues, respectively, we obtain the expression (see (Tsodyks et al., 1997))

$$2\lambda_{1,2} = \gamma_E(W_{EE}\Phi_E - 1) - \gamma_I(W_{II}\Phi_I + 1) \pm \sqrt{[\gamma_E(W_{EE}\Phi_E - 1) + \gamma_I(W_{II}\Phi_I + 1)]^2 - 4\gamma_E\gamma_I W_{EI}W_{IE}\Phi_E\Phi_I} \tag{52}$$

A gamma peak exists only if the expression under the square root is negative, *i.e.*

$$4\gamma_E\gamma_I W_{EI}W_{IE}\Phi_E\Phi_I > [\gamma_E(W_{EE}\Phi_E - 1) + \gamma_I(W_{II}\Phi_I + 1)]^2, \tag{53}$$

in which case, for the gamma peak angular frequency ω_0, we (approximately) have

$$4\omega_0^2 = 4\beta_E\beta_I W_{EI}W_{IE} - (\beta_E W_{EE} + \beta_I W_{II} + \gamma_I - \gamma_E)^2 \tag{54}$$

where we defined $\beta_X := \gamma_X\Phi_X$ for $X \in \{E, I\}$.

We will now obtain a simplified expression for the derivative of ω_0^2 with respect to the contrast c, using the rectified supralinear nonlinearity of the SSN. Using $\Phi_* = nk^{\frac{1}{n}} r_*^{1-\frac{1}{n}}$ (where r_* is the firing rate at fixed point) we obtain

$$\frac{d\beta_*}{dc} = \frac{n-1}{n}\beta_* \frac{d\ln r_*}{dc} \tag{55}$$

Then using Eq. (54), and defining

$$A := (\beta_E W_{EE} + \beta_I W_{II} + \gamma_I - \gamma_E) \tag{56}$$

and $(\cdots)' := \frac{d(\cdots)}{dc}$, we find:

$$\frac{n}{n-1}\frac{d\omega_0^2}{dc} = \beta_E\beta_I W_{EI}W_{IE}(\ln r_E + \ln r_I)' - \frac{2A}{4}\left(\beta_E W_{EE}(\ln r_E)' + \beta_I W_{II}(\ln r_I)'\right) \tag{57}$$

$$= \omega_0^2(\ln r_E + \ln r_I)' + \frac{1}{2}A^2\left[\frac{(\ln r_E)' + (\ln r_I)'}{2} - \frac{\sum_a w_a(\ln r_a)'}{\gamma_I - \gamma_E + \sum_a w_a}\right] \tag{58}$$

where the sums are over $a \in \{E, I\}$ and we defined

$$w_a := \beta_a W_{aa} \qquad a \in \{E, I\} \tag{59}$$

Analysis of the sign of $\frac{d\omega_0^2}{dc}$:

Assuming that we are in the gamma oscillatory regime (*i.e.*, ω_0 is real) and that the fixed point rates increase with contrast, then from Eq. (58) we find that sufficient conditoin for $\frac{d\omega_0^2}{dc} > 0$ is that the factor in the square brackets in Eq. (58) is positive. In the solutions of SSN most relevant to cortical biology, $(\ln r_I)'$ tends to be larger than $(\ln r_E)'$ (because excitatory rates tend to saturate or supersaturate earlier). We thus consider two extreme cases: $(\ln r_E)' = (\ln r_I)'$ and $(\ln r_E)' = 0$.

In the first case, the bracket becomes $(\ln r_I)'\left[1 - \frac{\sum_a w_a}{\gamma_I - \gamma_E + \sum_a w_a}\right] = (\ln r_I)'\frac{\gamma_I - \gamma_E}{\gamma_I - \gamma_E + \sum_a w_a}$, which is positive as long as $\gamma_I > \gamma_E$ (which is unfortunately not the case for GABA and AMPA).

In the second case, the bracket factor becomes $(\ln r_I)'\frac{\gamma_I - \gamma_E + \sum_a w_a - 2w_I}{2(\gamma_I - \gamma_E + \sum_a w_a)} = (\ln r_I)'\frac{\gamma_I - \gamma_E + w_E - w_I}{2(\gamma_I - \gamma_E + \sum_a w_a)}$. This is positive (as long as the denominator is positive, which is true as long as $\gamma_I > \gamma_E$) if

$$w_E - \gamma_E + \gamma_I > w_I \tag{60}$$

But the stability of the fixed point dictates that the expression on first line of Eq. (52) (the real part of the eigenvalues) has to be negative and thus

$$w_I > w_E - \gamma_E - \gamma_I. \tag{61}$$